Article

Not peer-reviewed version

Sulfonic DJ-1 (Cys^{106}-SO_3H) Binds to and Colocalizes with the Intracellular Accumulation of Amyloid-Beta 42 (Aβ42) in Familial Alzheimer's Disease PSEN1 E280A Cerebral Organoids Derived from Induced Pluripotent Stem Cells

Viviana Soto-Mercado , Miguel Mendivil-Perez , Carlos Velez-Pardo , Marlene Jimenez-Del-Rio *

Posted Date: 21 November 2025

doi: 10.20944/preprints202511.1634.v1

Keywords: Aβ42; Alzheimer; autophagy; DJ-1; ELISA; organoids; oxidative stress; induced pluripotent stem cells; sulfinic; sulfenic; sulfonic

 doi:10.20944/preprints202511.1634.v1

Article

Sulfonic DJ-1 (Cys^{106}-SO_3H) Binds to and Colocalizes with the Intracellular Accumulation of Amyloid-Beta 42 (Aβ42) in Familial Alzheimer's Disease PSEN1 E280A Cerebral Organoids Derived from Induced Pluripotent Stem Cells

Viviana Soto-Mercado [1], Miguel Mendivil-Perez [2], Carlos Velez-Pardo [1] and Marlene Jimenez-Del-Rio [1,*]

[1] Neuroscience Research Group, Institute of Medical Research, Faculty of Medicine, University of Antioquia, Calle 67 #53-108, University Research Headquarters, Calle 62#52-59, Building 1, Laboratory 411/412, and Medellin 050010, Colombia

[2] Neuroscience Research Group, Faculty of Nursing, University of Antioquia, Calle 67 #53-108, University Research Headquarters, Calle 62#52-59, Building 1, Laboratory 411/412, Medellin 050010, Colombia

* Correspondence: marlene.jimenez@udea.edu.co; Tel.: +57(4)-604-219-6457

Abstract

The intracellular accumulation of amyloid beta 42 (iAβ42) has been proposed as an early pathological indicator of familial Alzheimer's disease (FAD). DJ-1 is a multifunctional protein sensitive to oxidative stress (OS) that has been associated with neurodegeneration; however, its role in iAβ42 pathology is unclear. In this study, we examined whether oxidized (sulfonic) DJ-1 (Cys^{106}-SO_3) drives iAβ42 accumulation using postmortem brain samples and in vitro 3D (iPSC-derived cerebral organoids, COs) or 2D induced pluripotent stem cells (iPSC)-derived ChLNs (cholinergic-like neurons) models from a PSEN1 E280A patient and a healthy volunteer (as a control sample). Post-mortem analyses of the temporal and frontal cortices and hippocampus from FAD PSEN1 E280A patients revealed strong intracellular co-localization of sulfonic DJ-1 and iAβ42, which was absent in control samples. To validate these findings, we generated cerebral organoids (COs) from an iPSCs PSEN1 E280A FAD patient and a healthy donor. In these organoids, we observed the co-localization of oxidized DJ-1 and Aβ42 in the absence of extracellular fibrils or plaques, as confirmed by BTA-1 staining. To further support these observations, 2D iPSC PSEN1 E280A-derived ChLNs cultures showed that intracellular Aβ42 accumulates progressively in direct correlation with increasing DJ-1 oxidation, as demonstrated by immunofluorescence microscopy and Western blotting analysis. These results indicate that DJ-1 oxidation accompanies the earliest intracellular stages of Aβ42 pathology. Furthermore, complementary in silico molecular docking analysis revealed a higher affinity between Aβ42 and oxidized sulfonic DJ-1 (DJ-1 1Cys^{106}-SO_3) compared to sulfenic (DJ-1 Cys^{106}-SOH) or sulfinic acid (DJ-1 Cys^{106}-SO_2H) forms. Likewise, ELISA tests and seeding assays confirmed that oxidized DJ-1 binds to and decelerates Aβ42 aggregation kinetics. Together, our results identify DJ-1 oxidation as a critical molecular event in the accumulation of iAβ42 in FAD. These findings suggest that oxidized DJ-1 represents not only a potential early biomarker of intracellular pathology but also a pharmacological target. Preventing the oxidation of DJ-1 or its pathological aggregation could provide new biomarkers and therapeutic strategies for reducing the intracellular accumulation of Aβ42 and neurodegeneration in FAD.

Keywords: Aβ42; Alzheimer; autophagy; DJ-1; ELISA; organoids; oxidative stress; induced pluripotent stem cells; sulfinic; sulfenic; sulfonic

 doi:10.20944/preprints202511.1634.v1

1. Introduction

Familial Alzheimer's disease (FAD) is a genetically induced neurodegenerative condition characterized by early-onset dementia (onset before age 65) and a family history of dementia. It is also associated with various non-cognitive neurological symptoms and signs, as well as a more aggressive course [1,2]. Similar to sporadic Alzheimer's disease (SAD, [3]), FAD presents with abundant plaques composed of extracellular amyloid beta (eAβ), neurofibrillary tangles made of intracellular hyperphosphorylated tau protein (p-Tau), and loss of brain weight due to accelerated neuronal cell death. To date, at least 556 mutations in the presenilin (PSEN1 and PSEN2) and amyloid precursor protein (APP) genes have been identified in FAD (http://www.alzforum.org, accessed October 2025). These mutations affect a common pathogenic pathway in APP synthesis and proteolysis, leading to the excessive production of eAβ via a mechanism that is not yet fully understood [4]. PSEN1 is a key component of the aspartyl protease γ-secretase complex [5] and, together with β-secretase, preferentially cleaves APP (770 amino acids) at residues 713 and 671, respectively, producing an Aβ42 fragment [6]. Several hypotheses have been proposed to explain how eAβ42 induces AD and FAD. These include the amyloid cascade hypothesis [7], the cholinergic hypothesis [8], the oxidative stress hypothesis [9], the two-hit hypothesis [10], the mitochondrial hypothesis [11], the presenilin hypothesis [12], the inside-out amyloid hypothesis [13,14], the tau hypothesis [15], and the ApoE cascade hypothesis [16], among others [17,18]. However, none of these hypotheses have been proven conclusively, and some remain controversial (e.g., [19–22]. Therefore, the mechanism by which Aβ induces neurotoxicity and cell death is still open to validation.

Specifically, the intracellular amyloid hypothesis [23,24] posits that Aβ accumulation inside neurons, rather than just extracellular plaques, is an early driver of AD pathology, disrupting cellular functions like protein degradation, axonal transport, and cell survival. This accumulation can lead to tau hyperphosphorylation, neuronal dysfunction, and eventually cell death, making iAβ a promising therapeutic target. Consistent with this perspective, our research group has presented substantial evidence in support of the intracellular Aβ hypothesis. We have demonstrated that cholinergic-like neurons (ChLNs) with the E280A or the I416T mutation—which result from a substitution of aspartic acid (E) for alanine (A) at position 280 [25] or isoleucine (I) for threonine (T) at position 416 [26], respectively, —produce aberrant accumulation of iAβ, abnormal phosphorylation of tau, oxidative stress, mitochondrial depolarization, apoptosis, and calcium dysregulation [27,28]. Interestingly, we obtained PSEN1 E280A ChLNs derived from umbilical cord Wharton's jelly mesenchymal stromal cells (WJ-MSCs) or menstrual mesenchymal stromal cells (MenSCs), which are tissue equivalents [29], using the Cholinergic-N-Run medium (Ch-N-Rm, [30], and observed that by day 7 of the transdifferentiation process, mutant ChLNs exhibited abnormal accumulation of iAβ42, oxidized DJ-1 (i.e., DJ-1Cys^{106}-SO$_3$), which is indicative of oxidative stress (OS), and aberrant accumulation of autophagosomes. However, there was no evidence of cell death [27,31]. By day 11, however, cholinergic mutant cells exhibited abnormal phosphorylation of the protein TAU (at Ser^{202}/Thr^{205}) and positive markers of apoptosis, such as tumor protein p53 (TP53), p-Ser^{63}/Ser^{73} JUN, p53-upregulated modulator of apoptosis (PUMA), and cleaved caspase-3 (CC3). They also exhibited loss of mitochondrial membrane potential (ΔΨm) and dysfunctional acetylcholine (ACh)-induced Ca^{2+} ion influx [27]. These observations suggest that the accumulation of intraneuronal Aβ, oxidized DJ-1, and impairment of autophagy lysosomal pathway are early event in AD pathogenesis and precedes p-TAU and eAβ deposits [32]. Therefore, iA triggers signals that lead to neuronal dysfunction [33]. Because the earliest pathological detection in PSEN1 E280A ChLNs was the accumulation of iAβ and DJ-1Cys^{106}-SO$_3$ [27,31] and exposure to antioxidants, such as epigallocatechin-3-gallate and tramiprosate, simultaneously abolished the accumulation of iAβ and autophagosomes, and DJ-1 oxidation [31], this led us to wonder whether oxidized DJ-1 is essential to iAβ accumulation in mutant ChLN cells.

DJ-1 is a 189-amino-acid protein that is expressed throughout the body and forms dimers under physiological conditions. It is encoded by the *PARK7* gene, which was first associated with early-onset, familial forms of Parkinson's disease (FPD) [34]. As a homodimer protein [35], DJ-1 protects

 doi:10.20944/preprints202511.1634.v1

against oxidative stress (OS) by operating as an antioxidant, neuroprotectant, and survival signaling molecule [36]. DJ-1 can sense OS through thiolate Cys^{106}-SH residue, which is highly susceptible to oxidation by reactive oxygen species (ROS), particularly H_2O_2 [37,38]. Depending on the strength of intracellular oxidation, ranging from moderate to high, the thiolate Cys^{106}-SH can be oxidized into sulfenic form of DJ-1 (Cys^{106}-SOH), which can be oxidized to the sulfinic acid form (Cys^{106}-SO_2H) and then to the sulfonic acid form (Cys^{106}-SO_3H). The sulfinic DJ-1 form is responsible for DJ-1's neuroprotective actions [38–40]; whereas the sulfonic form is an unstable protein prone to aggregation and loss of function [41–43]. Interestingly, DJ-1 has been shown to undergo extensive and irreversible oxidation in the brains of patients with SAD [44,45]. Furthermore, Solti et al. [46] have shown that oxidized DJ-1 aggregates colocalize with pathological amyloid deposits in the postmortem brain tissue of human SAD patients. However, it is not yet known whether oxidized DJ-1 Cys^{106}-SO_3 colocalizes with iA in FAD postmortem brain tissue or in an in vitro model (e.g., organoids and 2D ChLNs culture).

To gain insight into these issues, we first sought to assess whether oxidized DJ-1, detected with rabbit recombinant monoclonal PARK7/DJ1 antibody, colocalizes with iAβ42 in the frontal and occipital cortex and hippocampus of PSEN1 E280A patients' postmortem and control brains. Next, we evaluated whether oxidized DJ-1 drives intracellular Aβ42 aggregation using 2D (iPSCs-derived ChLNs) and 3D in vitro models (iPSCs-derived organoids), and in silico molecular docking analysis together with ELISA test and fibril kinetics analysis.

2. Materials and Methods

2.1. Induced Pluripotent Stem Cells Reprogramming

One vial containing $1x10^6$ fibroblast cells (3rd passage) was thawed in one well of a 6-well plate previously treated with Vitronectin (VTN-N, Thermo Fisher Scientific, cat# A14700, Waltham, MA, USA). Once cells became >90% confluent were detached and split in 4 wells of a 6-well plate (1:4 ratio) in fibroblast medium, which include High glucose DMEM, (Thermo Fisher Scientific, cat# 11965092, Waltham, MA, USA), 10% Fetal Bovine Serum (Thermo Fisher Scientific, cat# A5256701, Waltham, MA, USA; 1X NEAA (Thermo Fisher Scientific, cat#11140050, Waltham, MA, USA), and 1X -mercaptoethanol (Thermo Fisher Scientific, cat#21985023, Waltham, MA, USA). On day 0 cells were transduced using the CytoTune™ 2.0 Sendai reprogramming (Thermo Fisher Scientific, cat# A16517, Waltham, MA, USA by incubating overnight with 10 l KOS, 10 l of hc-Myc, and 7 l hKlf4. After 1 day, the medium was replaced with fresh complete fibroblast medium to remove the CytoTune™ 2.0 Sendai reprogramming vectors, then after we changed the medium every other day, and once cells became >90% confluent they were detached and split in 3 wells of a 6-well plate. On day 7, the medium was changed to complete Essential 8™ Medium (Thermo Fisher Scientific, cat# A1517001, Waltham, MA, USA). On days 9–28 the medium was replaced every day and monitor the culture vessels for the emergence of iPSC colonies.

2.2. Neural Precursor Cell Generation Protocol

Human iPSC cells were mechanically detached from VTN-N surface. Embryoid bodies (EBs) were generated by transferring iPSCs to non-adherent plates in E6 medium (Thermo Fisher Scientific, cat# A1516401, Waltham, MA, USA) at 37 °C in 5% CO2. After 7 days, EBs were transferred to a non-adherent plate and E6 medium was supplemented with 10ng/ml bFGF (Thermo Fisher Scientific, cat# 100-18B-50UG, Waltham, MA, USA), after 2 days, the floating structures were dissociated by trituration and transferred to an VTN-N-treated dish. For generation of neural precursor cells (NPCs), EBs were cultured in NPC medium (Neurobasal medium, 1% N2 supplement, 2% B27 supplement (Thermo Fisher Scientific, cat# 17504044, Waltham, MA, USA), 20 ng/ ml epidermal growth factor (Thermo Fisher Scientific, cat#PHG0311L, Waltham, MA, USA), 1 g/ ml heparin sodium salt (Thermo Fisher Scientific, cat#A16198.MD, Waltham, MA, USA), 1ng/ ml bFGF, 1X -mercaptoethanol, and 1% penicillin/streptomycin (Thermo Fisher Scientific, cat#15140122, Waltham, MA, USA).

 doi:10.20944/preprints202511.1634.v1

2.3. Generation of Cholinergic Neurons from Neural Precursor Cells (NPCs)

Neural precursor cells (NPC) were seeded at a density of 3×10^4 cells/cm² in 24-well culture plates and maintained for 24 h in NPC culture medium under standard conditions. Following this period, the medium was replaced with a cholinergic differentiation medium (Cholinergic-N-Run, [30]), and cells were incubated at 37 °C for 7 days, as previously described [27]. After the induction phase, the differentiation medium was replaced with neural medium (NM) consisting of Neurobasal medium supplemented with 1×N2 (Thermo Fisher Scientific, cat#17502048, Waltham, MA, USA) and 1% penicillin/streptomycin.

2.4. Generation of Cerebral Organoids (COs)

Cerebral organoids (COs) were generated by differentiating wild-type (WT) and PSEN1 E280A mutant induced pluripotent stem cell (iPSC)-derived neural progenitor cells (NPCs), following the protocol described in ref. [29]. Briefly, WT and mutant NPCs were cultured in a novel medium formulation, *Fast-N-Spheres V2* [47], supplemented with Corning Matrigel® (Cat# 356232, Thermo Fisher Scientific Inc., Santa Fe, NM, USA) and 1% fetal bovine serum (FBS) (Cat# CVFSVF00-01, Eurobio Scientific, Les Ulis, France). Cells were maintained under standard conditions until the spontaneous formation of neurospheres was observed. Subsequently, the spheres were transferred to ultra-low attachment culture dishes and continuously agitated at 60 rpm. The culture medium was refreshed every 3–4 days, and organoids were maintained for a total of 60 days.

2.5. Western Blot Analysis

Cells were incubated as described above, detached with 0.25% trypsin, and lysed in 50 mM Tris-HCl, pH 8.0, with 150 mM sodium chloride, 1.0% Igepal CA-630 (NP-40), and 0.1% sodium dodecyl sulfate and a protease inhibitor cocktail (cat#P8340, Sigma-Aldrich Co. LLC, (USA)). All lysates were quantified using the bicinchoninic acid assay (Thermo Scientific cat # 23225, Waltham, MA, USA). Extracted samples (40 μg of proteins) were heated at 95 °C for 5 min in 2 x SDS and 20x reducing agent (except for protein oxDJ-1) and loaded into 12% Bis/Tris gels at 120 V for 90 min, and the bands were transferred onto nitrocellulose membranes (Hybond-ECL, Amersham Biosciences) at 270 mA for 90 min using an electrophoretic transfer system (BIO-RAD). The membranes were incubated overnight at 4 °C amyloid β1–42 and ox(Cys106) DJ1 primary antibodies (1:5000). The anti-actin antibody (1:1000, cat #MAB1501, Millipore) was used as an expression control. Secondary infrared antibodies (goat anti-rabbit IRDye® 680RD, cat #926–68071; donkey anti-goat IRDye ® 680RD, cat # 926–68074; and goat anti mouse IRDye ® 800CW, cat #926–32270; LI-CORBiosciences, Lincoln, NE, USA) at 1:1000 were used for western blotting analysis, and data were acquired using Odyssey software. The assessment was repeated three times in independent experiments.

2.6. Immunofluorescence Analysis

For the analysis of neural-, Alzheimer's disease-, oxidative stress- and cell death-related markers, the cells treated under different conditions were fixed with cold ethanol (-20 °C) for 20 min, followed by Triton X-100 (0.1%) permeabilization and 10% bovine serum albumin (BSA) blockage. Cells were incubated overnight with primary neural antibodies against OCT4 (1:500), SOX-2 (1:500), NANOG (1:500), and KLF4 (1:500), the neuronal marker Nestin (1:500; cat# MA1-5840, Invitrogen, Waltham, MA, USA); and glial fibrillary acidic protein (GFAP 1:200, cat# sc6170, Santa Cruz, Dallas, TX, USA), microtubule-associated protein 2 (MAP2, 1:250, cat MA1-25044, Invitrogen, Carlsbad, CA, USA), β-tubulin III (1:250, cat# G712 A, Promega, Madison, WI, USA) and choline-acetyltransferase (ChAT, 1:50, cat# AB144 P, Millipore, Burlington, MA, USA), amyloid β1–42 (1:500; clone 6E10, cat# 803014, Biolegend, San Diego, CA, USA), and primary antibodies against oxidized DJ-1 (1:500; ox(Cys^{106})DJ1; spanning residue C^{106} of human PARK7/DJ1; oxidized to produce cysteine sulfonic (SO_3) acid; cat #ab169520, Abcam, Cambridge, UK). After exhaustive rinsing, we incubated the cells with secondary fluorescent antibodies (DyLight 488 and 594 horse anti-rabbit, -goat and -mouse, cat

 doi:10.20944/preprints202511.1634.v1

DI 1094, DI 3088, and DI 2488, respectively) at 1:500. The nuclei were stained with 1 μM Hoechst 33342 (Life Technologies, Carlsbad, CA, USA), and images were acquired on a Floyd Cells Imaging Station microscope (Life Technologies, Carlsbad, CA, USA).

2.7. Flow Cytometry Analysis

For flow cytometry analyses, cells were detached using trypsin and centrifuged for 10 min at 2000 rpm. Then, cells were fixed using cold ethanol at -20 °C overnight. Then, cell suspensions were washed with PBS and incubated with 0.2% Triton X-100 plus 1.5% bovine serum albumin (BSA) for 30 min. After, cells were incubated with primary (see above). After exhaustive rinsing, we incubated the cells with secondary fluorescent antibodies (DyLight 488 and 594 horse anti-rabbit, -goat and -mouse, cat DI 1094, DI 3088, and DI 2488, respectively, Thermo Fisher Scientific, Waltham, MA, USA) at 1:500. Fluorescence analysis was performed on a BD LSRFortessa II flow cytometer (BD Biosciences, Becton, Dickinson and Company, BD Biosciences, 2350 Qume Dr, San Jose, CA 95131-1812, USA). Cells without primary antibodies served as a negative control. For assessment, 10,000 events and quantitative data and figures were obtained using FlowJo 7.6.2 Data Analysis Software (TIBCO® Data Science, Palo Alto, Ca, USA). Events analysis was performed by determining the cell population (Forward Scatter analysis, Y axis) that exceeded the basal fluorescence (488 nm or 594 nm, X axis) of the negative control. Accordingly, contour diagrams were created from event analysis, and the cells located in the box (quadrants labeled as + or (+)) represent the cell population exceeding the basal fluorescence.

2.8. Molecular Docking Analysis

To enable the 3D structure of DJ-1, the PDB database was used to access the PDB format of DJ-1 proteins under different oxidation status (Sulfenic, PDB:4p34; Sulfinic, PDB: 1soa; Sulfonic, PDB: 3bwe (aggregated)). Moreover, AlphaFold2.ipynb program (https://colab.research.google.com/github/sokrypton/ColabFold/blob/main/AlphaFold2.ipynb, accessed in July 2025) was loaded with the 42-aminoacid amyloid beta protein (Structured with AlphaFold2). The blind molecular docking was performed with HDOCK Server. For analysis, we selected the docking poses with the strongest Vina score. The generated PDB files of the molecular docking of each protein were visualized with the PDB viewer interphase.

2.9. Real-Time Quaking Induced Conversion (RT-QuIC)

Amyloid aggregation measurement was performed following minor modifications to a previously optimized protocol [48]. Purified DJ-1 protein was prepared at a concentration of 100 μg/mL in PBS, and 1 μg of protein was subsequently diluted in seeding buffer (PBS, pH 7.4). Synthetic Aβ42 peptide (100 μg/ml, Cat# ab120301, Abcam, Cambridge, UK,) was dissolved in DMSO (Cat#34869, Sigma-Aldrich Co. LLC, (USA)) and sonicated for 5 minutes immediately before the reaction. The peptide was then added to either untreated or H_2O_2 (100 μM) treated recombinant DJ-1 protein (Cat#P219-31H, Sino Biological, Beijing, China) in the presence of Congo Red (CR, 10 μM) in PBS. The final reaction volume for each mixture was 100 μL. Multiple technical replicates of each condition were incubated simultaneously in a Multiskan SkyHigh Plate Reader (Thermo Fisher Scientific, cat#A51119600DPC, Waltham, MA, USA) for 48 hours under intermittent shaking (600 rpm for 1 minute every 60 minutes) at 37 °C. Absorbance measurements were recorded every 60 minutes at 420 nm and 540 nm and used for subsequent analysis.

2.10. ELISA Test (Modified)

To determine the levels of oxidized DJ-1 (oxDJ-1) bound to $A\beta_{42}$ peptides, we designed a modified version of the Human $A\beta_{42}$ solid-phase sandwich ELISA (Cat. No. KHB3441, Invitrogen, Waltham, MA, USA). Briefly, recombinant DJ-1 protein (1 μg) was either left untreated or oxidized with H_2O_2 for 5 min. Each protein sample was then incubated with recombinant $A\beta_{42}$ peptide (1 μg)

 doi:10.20944/preprints202511.1634.v1

for 10 min. The resulting protein mixtures were subsequently used as substrates in the ELISA procedure. During the initial incubation step (in plate wells), the oxidized form of DJ-1 was detected using a specific anti-PARK7/DJ-1 antibody (oxidized cysteine sulfonic acid, Cat. No. ab169520, Abcam, Cambridge, UK) as the capture antibody. The remaining steps were performed according to the manufacturer's instructions. Binding levels were determined as the absorbance values after subtraction of the blank. This assay was conducted in triplicate in three independent experiments, with the experimenter blinded to sample identity.

2.10. Data Analysis

In this experimental design, two codes of iPSCs were cultured (WT PSEN1 and PSEN1 E280A) and the cell suspension was pipetted at a standardized cellular density of 2×10^4 cells/cm^2 into different wells of a 24- or 6-well plate. Cells (i.e., the biological and observational units) [49] were randomized to wells by simple randomization (sampling without replacement method), and then wells (i.e., the experimental units) were randomized to treatments by a similar method. Experiments were performed on three independent occasions (n = 3) blind to the experimenter and/or flow cytometer and/or microscopy analyst. The data from the three repetitions, i.e., independent experiments, were averaged, and representative flow cytometry density or histogram plots from the three independent experiments were selected for illustrative purposes, whereas the bars in the quantification figures represent the mean ± SD and the three black dots show the data point of each experimental repetition. Based on the assumptions that the experimental unit (i.e., the well) data comply with the independence of observations, the dependent variable is normally distributed in each treatment group (Shapiro–Wilk test), and there is homogeneity of variances (Levene's test), where the statistical significance is determined by a one-way analysis of variance (ANOVA) followed by Tukey's post hoc comparison calculated with GraphPad Prism 5.0 software. Differences between groups were only deemed significant with a p-value of 0.05 (*), 0.01 (**), and 0.001 (***). All data are presented as the mean ± S.D.

3. Results

3.1. A 42 and Sulfonic DJ-1 (Cys^{106}-SO$_3$H) Aggregates Colocalize in Familial Alzheimer's Disease (FAD) PSEN1 E280A Brain Samples

Because oxidized DJ-1 aggregates colocalize with pathological amyloid deposits in the postmortem brain tissue of human sporadic Alzheimer's disease (SAD) patients [46], we examined three regions of the brain: the hippocampus, the frontal and the occipital cortices. These regions are specifically involved in FAD caused by the PSEN1 E280A mutation [50], as well as in control cases. Immunohistochemical analysis revealed no reactivity of specific monoclonal antibodies (e.g., E610) against Aβ42 or sulfonic DJ-1 (SO_3H) in the wild-type (WT) PSEN1 hippocampus (**Figures 1A–C and 1A′–C′**), frontal cortex (**Figures 1H–J and 1H′–J′**), and occipital cortex (**Figures 1O–Q and 1O′–Q′**). However, evident oxDJ-1 (Cys^{106}) and Aβ42 fluorescent aggregates were detected in the PSEN1 E280A hippocampus (**Figures 1D–F**), frontal cortex (**Figures 1K–M**), and occipital cortex (**Figures 1R–T**). A close examination revealed that oxDJ-1 (Cys^{106}) and Aβ42 aggregates colocalize in PSEN1 E280A samples (**Figures 1D′-F′, 1K′-M′, and 1R′-T′**). Overall, PSEN1 E280A exhibited higher intracellular colocalization levels than control samples in the hippocampus (**Figure 1G**), frontal cortex (**Figure 1N**), and occipital cortex (**Figure 1U**).

 doi:10.20944/preprints202511.1634.v1

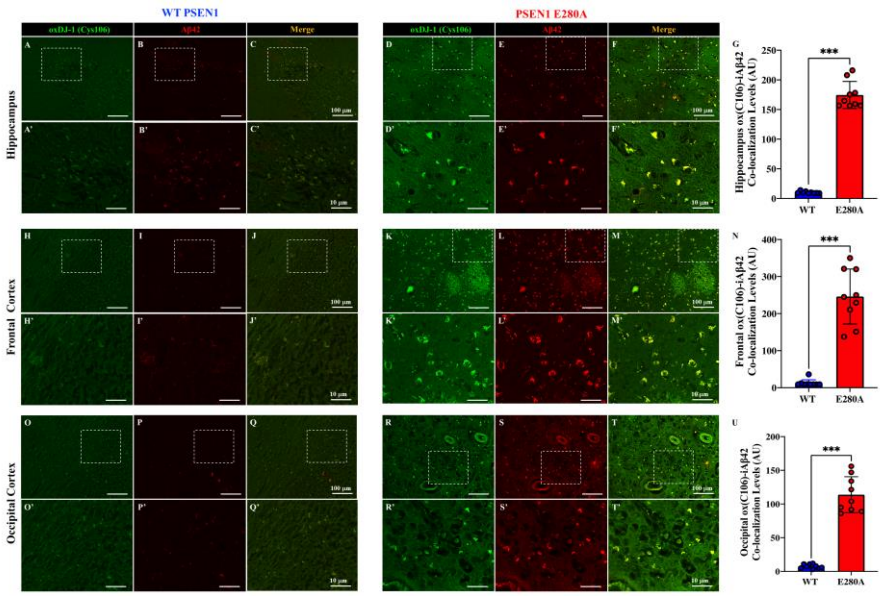

Figure 1. DJ-1 oxidation co-localizes with amyloid beta 42 (A 42) reactivity in postmortem cerebral slides from familial Alzheimer's disease PSEN1 E280A individuals. Hippocampal (A-F and A′-F′ insets), Frontal cortex (H-M and H′-M′ insets) and Occipital cortex (O-T and O′-T′ insets) representative pictures showing oxidized oxDJ-1(Cys^{106}) (A, D, H, K, O and R), A 42 aggregates (B, E, I, L, P and S) and merge (C, F, J, M, Q and T) labelling in WT (A-C, H-J, and O-Q) and PSEN1 E280A (D-F, K-M, and R-T) with anti-DJ-1 monoclonal antibody against cysteine^{106} sulfonic (SO_3) and anti-amyloid β1–42 antibody 6E10. Images were analyzed and quantitative data for protein co-localization was compared (G, N and S). Data are expressed as mean ± SD; *** $p < 0.001$. Photomicrographs, figures, and bars represent 1 of 3 WT PSEN1 individuals and 1 of 5 PSEN1 E280A cases. Image magnification ×10. Inset magnification ×100 is a representation of broken lines square.

3.2. Intracellularly, Aggregated Sulfonic DJ-1 (Cys^{106}-SO_3H) Colocalized with Aggregated Aβ42 in PSEN1 E280A Cerebral Organoids (COs).

Next, we investigated whether sulfonic DJ-1 (Cys^{106}-SO_3H) and intracellular Aβ42 could colocalize in cerebral organoids, which serve as a model of familial Alzheimer's disease (FAD). To achieve this aim, we first generated induced pluripotent stem cell (iPSC)-derived cerebral organoids (COs). **Figure 2** shows time-lapse microphotographs of iPSC transformation into COs from wild-type (WT) (**Figures 2A–D**) and PSEN1 E280A (**Figures 2E–H**) cells from day 0 to 20. Light microscopy analysis shows no significant morphological alterations in WT or mutant COs. Therefore, we selected day 20 to evaluate the expression of the neuronal marker MAP2, the cholinergic lineage marker ChAT, and the astrocyte lineage marker GFAP (**Figures 2I and 2J**). We observed that the three markers were readily expressed in both WT (**Figures 2I′-2III‴**) and mutant (**Figures 2J′-2J‴**) COs. Overall, there was no statistical difference in the expression of the MAP2 (**Figure 2K**), ChAT (**Figure 2L**), and GFAP (**Figure 2M**) markers between WT and PSEN1 E280A COs. The cultures were then left to progress until day 50. Time-lapse microphotographs from days 25 to 50 show no morphological changes (**Figures 2N–U**) or statistically significant differences in diameter length between WT and PSEN1 E280A COs (**Figure 2V**). Therefore, we inferred that the PSEN1 E280A mutation does not alter the normal development of iPSC-derived COs (**Figures 2A–V**).

 doi:10.20944/preprints202511.1634.v1

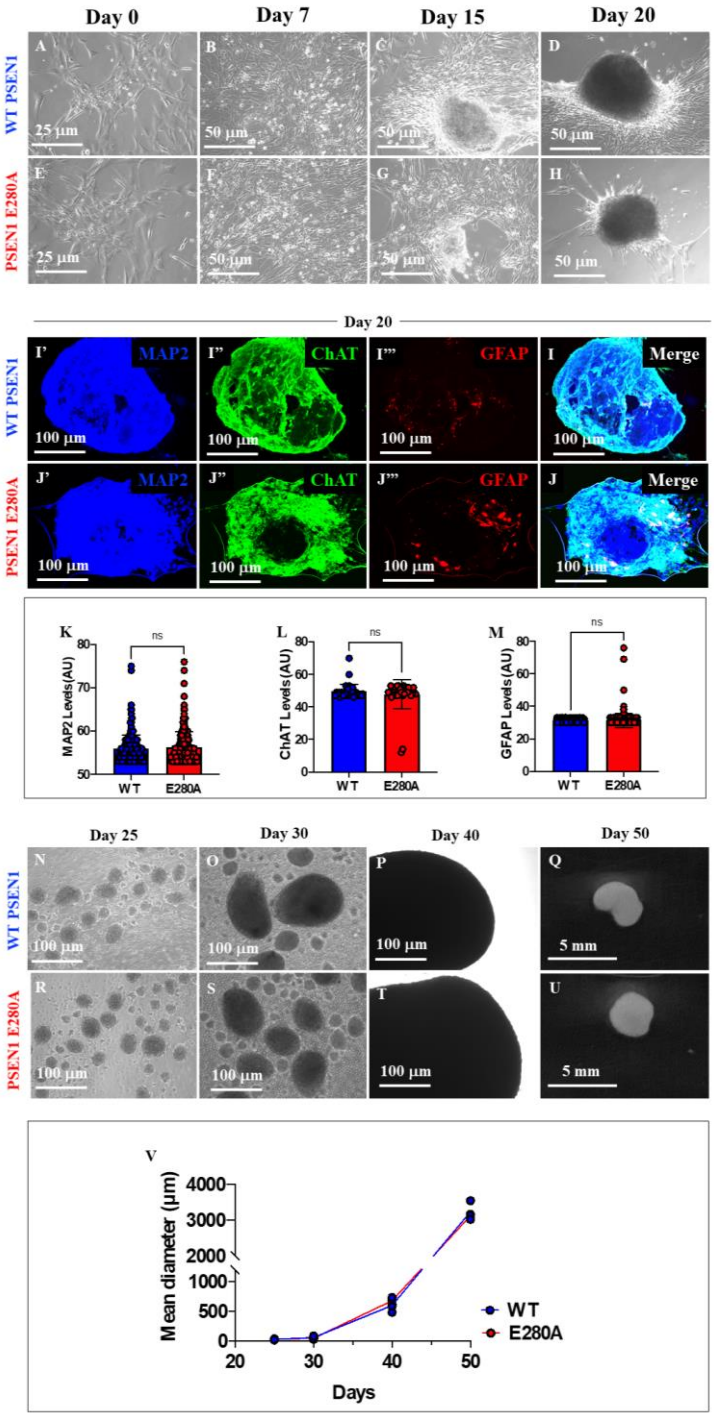

Figure 2. Generation of organoids from WT PSEN1 and PSEN1 E280A iPSC-derived neural precursor cells (NPC). WT PSEN1 and PSEN1 E280A NPCs were cultivated as described in Materials and Methods section and spontaneous organoid formation was noticed. Representative light images showing 0 (A, E), 7 (B, F), 15 (C, G) and 20 (D, H) days of organoids progression from WT PSEN1 individual's- (A-D) and PSEN1-E280A (E-H) patient's-derived NPC. Representative fluorescence images showing the MAP2 (blue; I', J'), ChAT (red; I'', J''), GFAP (red; I''', J''') and merge (I, J) labelling of WT (I'-I) and PSEN1-E280A (J'-J) organoids after 20 days. Images were analyzed and quantitative data for MAP2 (K), ChAT (L) and GFAP (M) was compared. Representative light images showing 25 (N, R), 30 (O, S), 40 (P, T) and 50 (Q, U) days of organoids progression from WT PSEN1 individual's- (N-Q) and PSEN1-E280A (R-U) patient's-derived NPC. Comparative analysis of organoids diameter (V). Data are expressed as the mean ± SD; ns= not significant. Light images magnification (A-H), 10x. Fluorescence Images magnification, 10x. Light images magnification (N-P; R-T), 5x.

 doi:10.20944/preprints202511.1634.v1

Further analysis was performed to detect the presence of iAβ42 and oxidized DJ-1 in COs on day 20. As expected, wild-type (WT) COs showed almost no iAβ42 or oxidized DJ-1 (**Figure 3A and the inset**), whereas PSEN1 E280A COs conspicuously expressed iAβ42 (**Figure 3B' and the inset**) and oxidized DJ-1 (**Figure 3B''**). Interestingly, oxDJ-1 colocalized with Aβ42 in mutant COs, showing a significant increase in oxDJ-1 (**Figure 3C**), iAβ42 (**Figure 3D**), and a higher colocalization ratio in PSEN1 COs (**Figure 3E**).

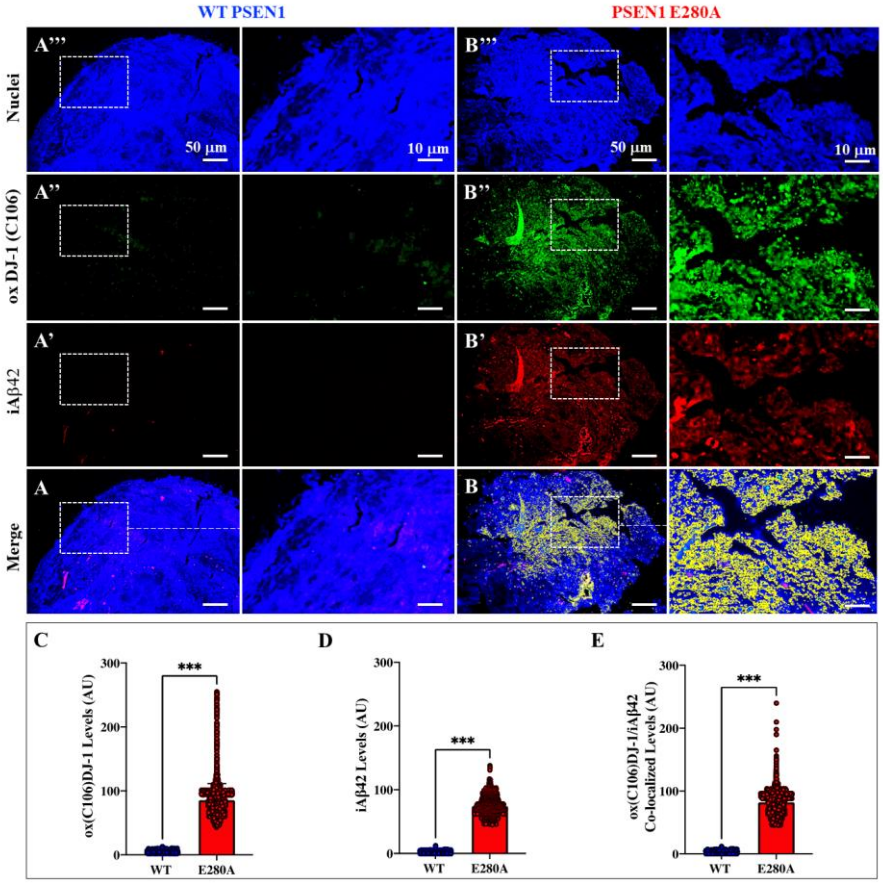

Figure 3. Cerebral organoids derived from PSEN1 E280A neural precursor cells (NPC) show intracellular Aβ42 colocalization with sulfonic DJ-1(Cys^{106}-SO$_3$H). WT PSEN1 and PSEN1 E280A NPC were cultivated in as described in Materials and Methods section to induce spontaneous organoid formation. After 60 days, organoids were collected and immunofluorescence analysis was performed. Representative fluorescence images showing nuclei (A, B and insets), oxDJ-1 (Cys^{106}-SO$_3$H) (A'', B'' and insets), iA 42 (A', B' and insets) and oxDJ-1(Cys^{106}) /iA 42 co-localization (A, B, and insets) in WT PSEN1 and PSEN1 E280A organoids. Images were analyzed and quantitative data for oxDJ-1(Cys^{106}) (C), iA 42 (D), and oxDJ-1(Cys^{106}) /iA 42 co-localization (E). Data are expressed as the mean ± SD; ***p<0.001. The figures represent one of three independent experiments. Fluorescence Images magnification, 10x.

To confirm that the colocalization of A 42 and OxDJ-1 aggregates was intracellular and not due to Aβ plaques and oxidized DJ-1 [46], we stained COs or postmortem tissue samples (as controls) with BTA-1, which is a probe for β-amyloid aggregates or A plaques. Figure 4 shows that neither WT (Figure 4A) nor PSEN1 E280A COs (Figure 4B) stain positive for BTA-1 (Figure 4C). In contrast, while post-mortem negative control brain sample showed none BTA-1 stain reactivity (Figure 4D), PSEN1 E280A showed abundant A plaques as stained in pink fluorescence (Figure 4E and 4F).

 doi:10.20944/preprints202511.1634.v1

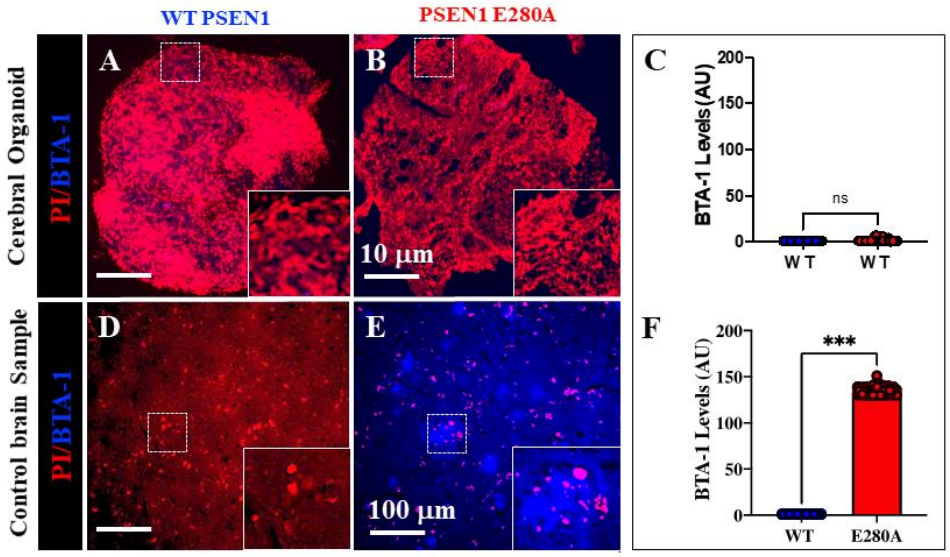

Figure 4. Increased intracellular Aβ42 and oxidized DJ-1 (Cys^{106}-SO_3H) precede fibril and plaque formation in cerebral organoids derived from PSEN1 E280A neural precursor cells. WT PSEN1 and PSEN1 E280A NPC were cultivated as described in Materials and Methods section to induce spontaneous organoid formation. After 60 days, organoids were collected, and fluorescence analysis was performed. Representative fluorescence images showing nuclei (red) and BTA-1 A 42 staining (blue) in WT PSEN1 (A) and PSEN1 E280A (B) organoids. Images were analyzed and quantitative data for BTA-1 A 42 staining (C) was compared. Representative fluorescence images showing Nuclei (red) and BTA-1 A 42 staining (blue) in WT PSEN1 (D) and PSEN1 E280A (E) cerebral slices. Images were analyzed and quantitative data for BTA-1 A 42 staining (F) was compared. Data are expressed as the mean ± SD; ***p<0.001; ns= not significant. The figures represent one of three independent experiments. Fluorescence Images magnification, 10x.

3.3. Intracellularly, Aggregated Sulfonic DJ-1 (Cys^{106}-SO_3H) Colocalized with Aggregated Aβ42 in PSEN1 E280A Cholinergic Neurons (ChNs).

To further refine our investigation of intracellular Aβ42-DJ-1 colocalization at the cellular level, we obtained cholinergic neurons (ChNs) from induced pluripotent stem cell (iPSC)-derived neural precursor cells (NPCs). Figures 5A–F illustrate the progressive development of fibroblast-derived iPSCs in wild-type (WT) and PSEN1 E280A cells over the course of three time points: day 1 (Figures 5A and 5B), day 7 (Figures 5C and 5D), and day 28 (Figures 5E and 5F). The iPSC colonies were noticeable by day 7 in the wild-type (WT) cells (Figure 5C, indicated by a blue broken circle) and in the PSEN1 E280A mutant cells (Figure 5D, indicated by a red broken circle). Additional analysis of pluripotency markers using the immunofluorescence technique revealed that both the WT and PSEN1 E280A fibroblast-derived iPSCs readily expressed OCT4 and SOX2 (Figures 5G and 5I), as well as NANOG and KLF4 (Figures 5H and 5J), respectively. There was no statistical difference in pluripotency marker expression between WT and PSEN1 E280A iPSCs (Figure 5K). Similar results were obtained using flow cytometry analysis (Figures 5L–N). The induced pluripotent stem cell (iPSC)-derived wild-type (WT) (Figure 5O) and PSEN1 E280A (Figure 5P) embryoid bodies (EBs) and cells obtained by dissociation (Figure 5Q and 5R) expressed Nestin, a widely used marker for neural stem and progenitor cells (NSPCs), and SOX2, a neuronal lineage marker, in both WT (Figure 5S) and PSEN1 E280A (Figure 5T). There was no statistical difference in Nestin or SOX2 expression between WT and PSEN1 E280A iPSCs (Figure 5K). Similar results were obtained via flow cytometry analysis (Figures 5V and 5W).

 doi:10.20944/preprints202511.1634.v1

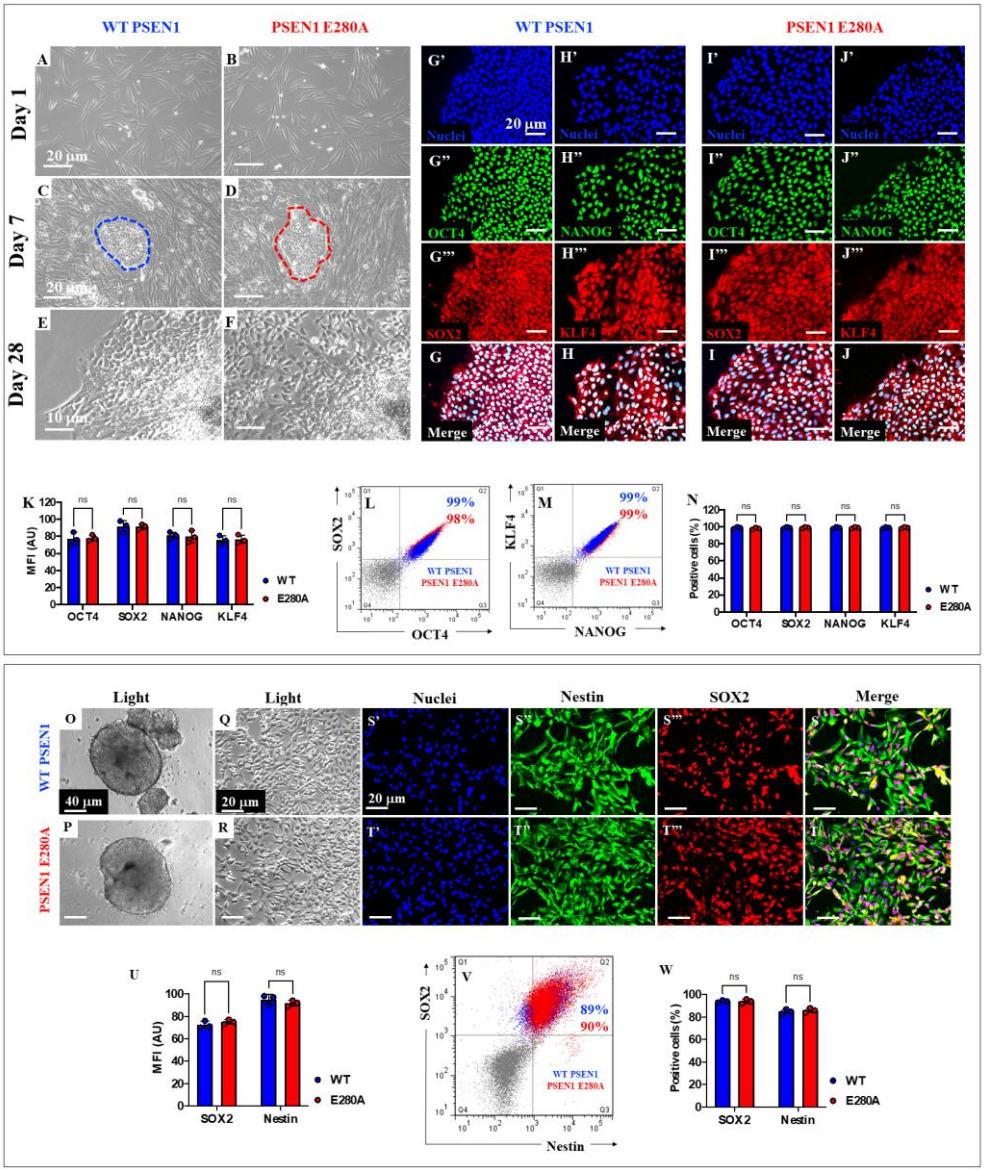

Figure 5. Induced-Pluripotent Cells (iPSC) and immediate Neural Precursor Cells (NPC) generation from WT PSEN1 (control) individual's- and PSEN1-E280A patient's-derived fibroblasts. Representative light images showing 1 (A, B), 7 (C, D) and 28 (E, F) days emerging iPSC colonies from WT PSEN1 healthy (control) individual (A, C, E) and PSEN1 E280A (B, D, F) patient's-derived fibroblasts. Determination of pluripotency markers by immunofluorescence. Nuclear (G'-J') colocalization of OCT4 (G'' and I'') and SOX2 (G'''and I''') in WT (G) and PSEN1 E280A (I) iPSC. Colocalization of NANOG (H'' and J'') and KLF4 (H''' and J''') in WT (H) and PSEN1-E280A (J) iPSC. Images were analyzed and quantitative data was compared (K). Flow cytometry analysis of negative controls (gray dot plots), WT (blue dot plots) and PSEN 1 E280A (red dot plots) iPSC to identify SOX2/OCT4 (L) and NANOG/KLF4 (M) double positive cells. Quantitative data showing the mean percentage of OCT4, SOX2 NANOG and KLF4 positive iPSC (N). Representative light images showing WT (O) and PSEN 1 E280A (P) iPSC-derived embryoid bodies. Representative light images showing WT (Q) and PSEN 1 E280A (R) embryoid bodies-derived NPC. Determination of Neural Stem Cells markers by immunofluorescence. Nuclei staining (S'-T') and identification of Nestin (S'', T'') and SOX2 (S''', T''') in WT (S) and PSEN1-E280A (T) NPC. Images were analyzed and quantitative data was compared (U). Flow cytometry analysis of negative controls (gray dot plots), WT (blue dot plots) and PSEN 1 E280A (red dot plots) NPC to identify Nestin/SOX2 (V) double positive cells. Quantitative data showing the mean percentage of Nestin and SOX2 positive NPC (W). Data are expressed as mean ± SD; ns = not significant. Photomicrographs, figures, and bars represent one out of three independent experiments. Light images magnification 10x. Fluorescence images magnification 20x.

 doi:10.20944/preprints202511.1634.v1

The NPC-derived wild-type (WT) (Figure 6A) and NPC-derived PSEN1 E280A (Figure 6E) cholinergic neurons (ChNs) expressed β-III tubulin, the earliest marker of neuronal differentiation (Figures 6B and 6F), as well as ChAT, a specific cholinergic marker (Figures 6C and 6G). However, they expressed low levels of the astrocyte marker GFAP (Figures 6D and 6H). No statistical difference was observed in β-III tubulin, ChAT, and GFAP expression between NPC-derived WT and PSEN1 E280A ChNs (Figure 6I). Similar results were obtained via flow cytometry analysis (Figures 6J, 6K, and 6L). Previous studies have shown that the earliest pathological markers found in ChLNs are iAβ42 and oxidized DJ-1 (Cys^{106}-SO_3) on day 0 (day 7 after transdifferentiation) [27,31]. Here, we extend this observation to include days 2 and 4 (days 9 and 11 after transdifferentiation). Western blot analysis revealed that WT ChNs showed no detectable iAβ42 or ox-DJ-1 at any evaluated time point (Figure 6M). However, PSEN1 E280A ChNs expressed iAβ42 and ox-DJ-1 in a time-dependent manner (Figure 6N). Moreover, both iAβ42 or ox-DJ-1 aggregates significantly increase in PSEN1 E280A ChNs compared to WT ChNs (Figures 6O and 6P). Similar results were obtained by immunofluorescence microscopy analysis (Figure 6Q-Y).

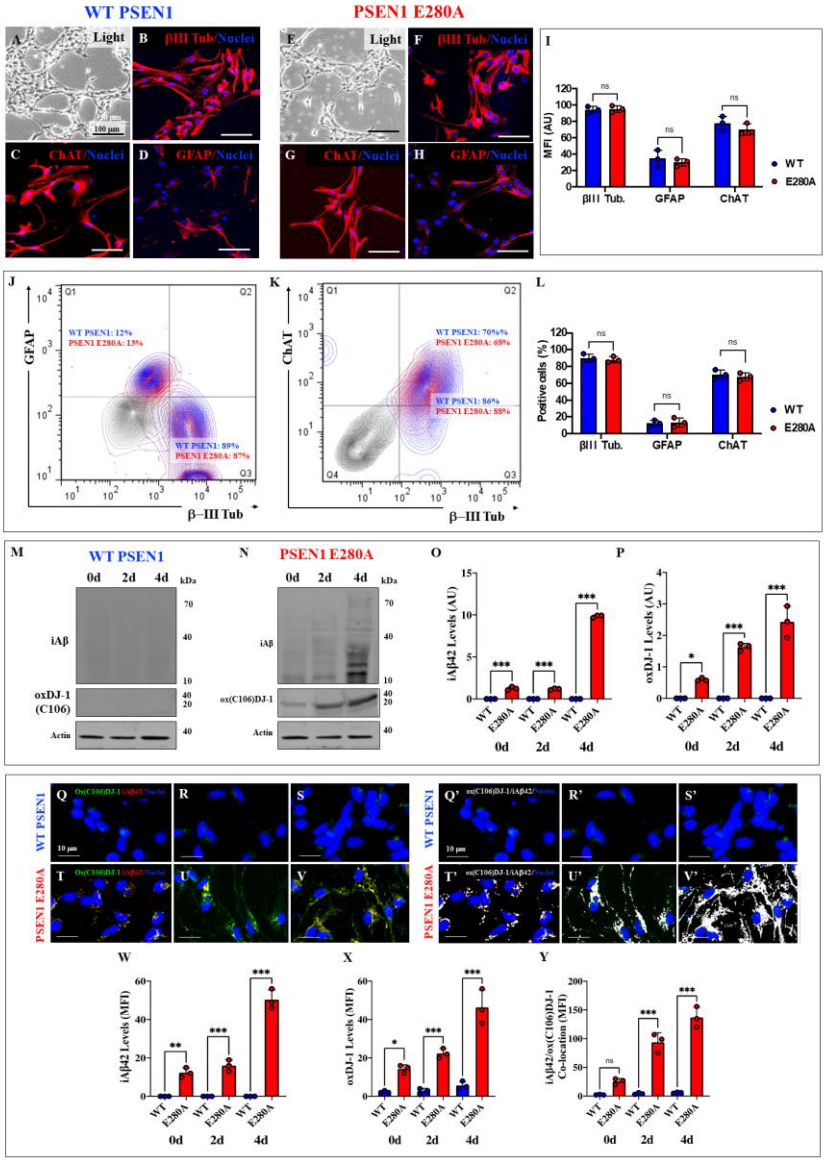

Figure 6. PSEN1 E280A Cholinergic neurons (ChN) show increasing levels of intracellular Aβ42 and oxidized DJ-1 (Cys^{106}) upon differentiation. Representative light images showing 7 days differentiated neurons from NPC-derived WT PSEN1 (A) and PSEN1 E280A ChNs (E). Determination of neural markers by immunofluorescence. Nuclear (blue) and III Tubulin (red) labelling of WT (B) and PSEN1-E280A neural cells (F). Nuclear (blue) and ChAT (red) labelling of WT (C) and PSEN1-E280A (G). Nuclear (blue) and GFAP (red) labelling of WT (D) and

 doi:10.20944/preprints202511.1634.v1

PSEN1-E280A (H). Images were analyzed and quantitative data was compared (I). Flow cytometry analysis of negative controls (gray dot plots), WT (blue dot plots) and PSEN 1 E280A (red dot plots) ChN to identify III Tubulin/GFAP (J) and III Tubulin/ChAT (K) double positive cells. Quantitative data showing the mean percentage of III Tubulin, GFAP, and ChAT positive ChN (L). After 7 days of differentiation, WT PSEN1 and PSEN1 E280A ChNs were left in neural medium (NM) for 0, 2, and 4 days post-transdifferentiation, as indicated in the figure. After this time, the proteins in the extracts were blotted with primary antibodies against Aβ42, ox DJ-1 (Cys^{106}) and actin proteins. The intensities of the western blot bands shown in (M and N) were measured (O, P) by an infrared imaging system (Odyssey, LI-COR), and the intensity was normalized to that of actin. Additionally, WT PSEN1 (Q-S) and PSEN1 E280A (T-V) ChNs were double stained as indicated in the figure with primary antibodies against ox(Cys^{106}) DJ-1 (green) and iAβ42 (red). The nuclei were stained with Hoechst 33342 (blue). The ox(Cys^{106}) DJ-1 (green) and Aβ42 (red) was further co-localized as shown in figures (Q'-V') Quantification of iAβ42 fluorescence intensity (W). Quantification of ox(Cys^{106}) DJ-1 fluorescence intensity (X). Quantification of iAβ42/ox(C106) DJ-1 fluorescence co-localization (Y). Data are expressed as the mean ± SD; *p<0.05; **p<0.01; ***p<0.001; ns= not significant. The blots and figures represent one of three independent experiments. Light images magnification, 10x. Fluorescence Images magnification in (B-D and F-H), 20x. Fluorescence Images magnification in (Q-V and Q'-V'), 40x**.**

3.4. Sulfonic DJ-1 (Cys^{106}-SO_3H) Protein Binds A 42 More Efficiently than Sulfenic DJ-1 (Cys^{106}-SOH) or than Sulfinic DJ-1 (Cys^{106}-SO_2H) In Vitro

The above observations prompted us to evaluate the molecular interactions between the Aβ42 peptide and the DJ-1 protein. In silico molecular docking analysis showed that DJ-1 binding to monomeric Aβ42 depends on the oxidative state of the DJ-1 protein. Theoretical calculations predict an increase in binding affinity from sulfenic DJ-1 (DS: -195.81 **Figure 7A**) to sulfinic DJ-1 (DS: -203.03, **Figure 7B**) to aggregated sulfonic DJ-1 (DS: -228.94, **Figure 7C**) in the presence of monomeric Aβ42 (**Table 1**). Sulfonic DJ-1 (aggregated) displayed more receptor-ligand interface residue pairs with Aβ42 (e.g., 75) than sulfenic (e.g., 43) or sulfinic DJ-1 (e.g., 45). Overall, sulfonic DJ-1 (aggregated) efficiently forms a protein complex with Aβ42 with 70% affinity folds (bonding residues) compared to sulfenic or sulfinic DJ-1. To verify the binding of sulfonic DJ-1 with Aβ42, we performed an ELISA assay (**Figures 7D and 7E)** and real-time quaking-induced conversion (RT-QuIC) experiments. In the absence of H_2O_2 (**Figures 7D and 7F)**, the ratio of sulfonic DJ-1 binding to A 2 was extremely low, whereas in the presence of H_2O_2, the binding ratio increased 28-folds (**Figure 7E and 7F**). In the absence of H_2O_2 (**Figure 7G)**, the RT-QuIC analysis revealed that synthetic Aβ42 underwent fibrillar elongation, which was characterized by in a lag phase (0–5 h, 0-20% CR relative absorbance). This phase represents the time at which sub-detectable growth of or initial growth of Aβ seeds occurs. The analysis also revealed an exponential growth phase (5–9 h, 20-90% CR), which represents the time at which detectable Aβ42 fibril growth occurs and generation of new seeding surfaces by fibril fragmentation and/or secondary nucleation. Finally, the analysis revealed a plateau phase (9–48 h, 70-90% CR), which reflects the exhaustion of available Aβ42. Under H_2O_2 exposure (**Figure 7H**), the CR50% was almost unaltered for both conditions; however, sulfonic DJ-1 significantly reduced typical $Aβ_{42}$ fibrillar growth, primarily during the plateau phase (**Figure 7H**). This reduction occurred from an initial CR relative absorbance of almost 90% (A 42 as control) to ~70% by 9-48 h, representing a -22% decrease in Aβ42 CR relative absorbance.

Table 1. *In silico* molecular docking analysis of Aβ42 (synthetized with AlphaFold2), Sulfenic (PDB: 4p34), Sulfinic (PDB: 1soa), and Sulfonic (PDB: 3bwe, aggregated) DJ-1 according to HDOCK Server. *Abbreviations*: RMSD, root mean square deviation.

Sulfenic DJ-1 (PDB:4p34)	**Sulfinic DJ-1 (PDB: 1soa)**	**Sulfonic DJ-1 (aggregated) (PDB: 3bwe)**
Rank 1 Docking Score **-195.81**	Rank 1 Docking Score **-203.03**	Rank 1 Docking Score **-228.94**

 doi:10.20944/preprints202511.1634.v1

Confidence Score 0.7143 Ligand RMSD (Å) 46.53	Confidence Score 0.7428 Ligand RMSD (Å) 57.22	Confidence Score 0.8290 Ligand RMSD (Å) 55.45
# Receptor-ligand interface residue pair(s):	# Receptor-ligand interface residue pair(s):	# Receptor-ligand interface residue pair(s):
10A - 6A 4.346	15A - 14A 4.879	459C - 28A 4.523
19A - 6A 4.299	16A - 14A 2.546	480C - 34A 3.873
20A - 6A 4.622	17A - 12A 4.611	481C - 31A 4.885
23A - 6A 3.948	17A - 14A 3.218	483C - 34A 4.134
23A - 8A 3.013	20A - 36A 4.581	483C - 40A 4.263
24A - 8A 3.794	23A - 35A 4.561	484C - 31A 3.222
24A - 10A 3.362	23A - 37A 4.079	484C - 32A 2.234
27A - 6A 4.357	24A - 36A 3.589	484C - 33A 3.308
27A - 8A 2.804	24A - 37A 2.763	484C - 34A 3.539
27A - 9A 4.734	24A - 38A 4.702	484C - 40A 4.888
27A - 10A 4.287	25A - 37A 4.974	484C - 42A 4.769
28A - 10A 2.819	27A - 35A 3.330	485C - 31A 4.524
28A - 12A 3.467	27A - 37A 2.510	485C - 32A 4.720
28A - 14A 3.985	27A - 38A 4.167	485C - 42A 4.433
29A - 14A 4.540	27A - 39A 3.233	486C - 32A 4.082
35A - 6A 3.233	28A - 37A 3.705	486C - 42A 3.537
43A - 2A 2.628	32A - 41A 4.286	489C - 41A 4.013
50A - 4A 4.620	35A - 35A 3.981	489C - 42A 3.431
51A - 1A 3.923	43A - 19A 4.337	513C - 38A 2.959
51A - 2A 3.984	49A - 16A 3.007	513C - 39A 3.341
51A - 3A 3.947	50A - 14A 2.902	514C - 34A 4.620
51A - 4A 2.667	50A - 15A 4.585	514C - 39A 3.644
51A - 5A 4.470	50A - 16A 3.969	514C - 40A 2.518
52A - 4A 3.056	50A - 17A 4.890	514C - 41A 4.176
52A - 5A 4.684	51A - 16A 2.594	515C - 40A 4.404
52A - 6A 2.027	51A - 17A 2.518	516C - 39A 4.090
53A - 2A 4.128	51A - 18A 4.384	516C - 41A 3.567
53A - 3A 4.738	52A - 17A 4.577	519C - 39A 4.988
53A - 4A 3.229	52A - 35A 3.863	532C - 38A 4.257
53A - 5A 3.217	53A - 17A 4.955	535C - 37A 2.320
53A - 6A 3.879	53A - 19A 3.666	535C - 38A 3.457
55A - 6A 4.663	53A - 35A 2.906	538C - 39A 4.369
176A - 16A 4.862	54A - 35A 4.366	944E - 16A 3.351
177A - 14A 3.654	55A - 35A 3.855	945E - 12A 3.080
180A - 14A 3.227	145A - 6A 3.860	945E - 13A 3.850
180A - 16A 4.505	145A - 8A 4.942	945E - 14A 4.000
181A - 14A 3.030	159A - 8A 4.745	958E - 11A 4.961
183A - 35A 4.276	162A - 10A 3.385	959E - 11A 3.619
183A - 36A 3.129	185A - 10A 2.484	959E - 13A 4.179

 doi:10.20944/preprints202511.1634.v1

183A - 37A	2.898	
184A - 36A	3.513	
184A - 37A	4.304	
186A - 37A	3.375	
186A - 10A	3.138	
187A - 10A	3.307	
188A - 4A	3.685	
188A - 5A	2.875	
188A - 6A	4.524	
188A - 7A	2.336	
960E - 13A	4.972	
961E - 13A	4.961	
962E - 11A	4.542	
962E - 13A	2.584	
963E - 12A	4.458	
963E - 13A	2.822	
963E - 14A	3.253	
963E - 15A	4.058	
966E - 15A	2.898	
967E - 15A	4.795	
982E - 15A	3.787	
987E - 11A	4.478	
987E - 13A	3.121	
988E - 10A	3.976	
988E - 11A	2.251	
988E - 12A	2.977	
988E - 13A	3.568	
989E - 11A	4.919	
989E - 13A	3.650	
989E - 36A	3.876	
1145F - 9A	4.393	
1145F - 10A	3.298	
1145F - 11A	3.206	
1146F - 7A	4.489	
1148F - 3A	3.615	
1149F - 3A	4.950	
1150F - 3A	3.420	
1159F - 11A	3.634	
1159F - 13A	4.968	
1162F - 11A	3.490	
1163F - 7A	4.202	
1163F - 9A	2.380	
1163F - 10A	3.867	
1163F - 11A	3.638	
1166F - 7A	4.566	
1167F - 7A	3.239	
1170F - 5A	2.632	
1170F - 6A	3.503	
1170F - 7A	4.109	
1171F - 5A	4.242	
1174F - 5A	3.650	
1175F - 5A	4.306	
1175F - 6A	4.137	
1182F - 8A	3.585	

 doi:10.20944/preprints202511.1634.v1

		1182F - 9A 4.474 1187F - 11A 3.026 1188F - 10A 3.195 1188F - 11A 4.233 1188F - 12A 1.940 1188F - 13A 3.895 1188F - 14A 4.424

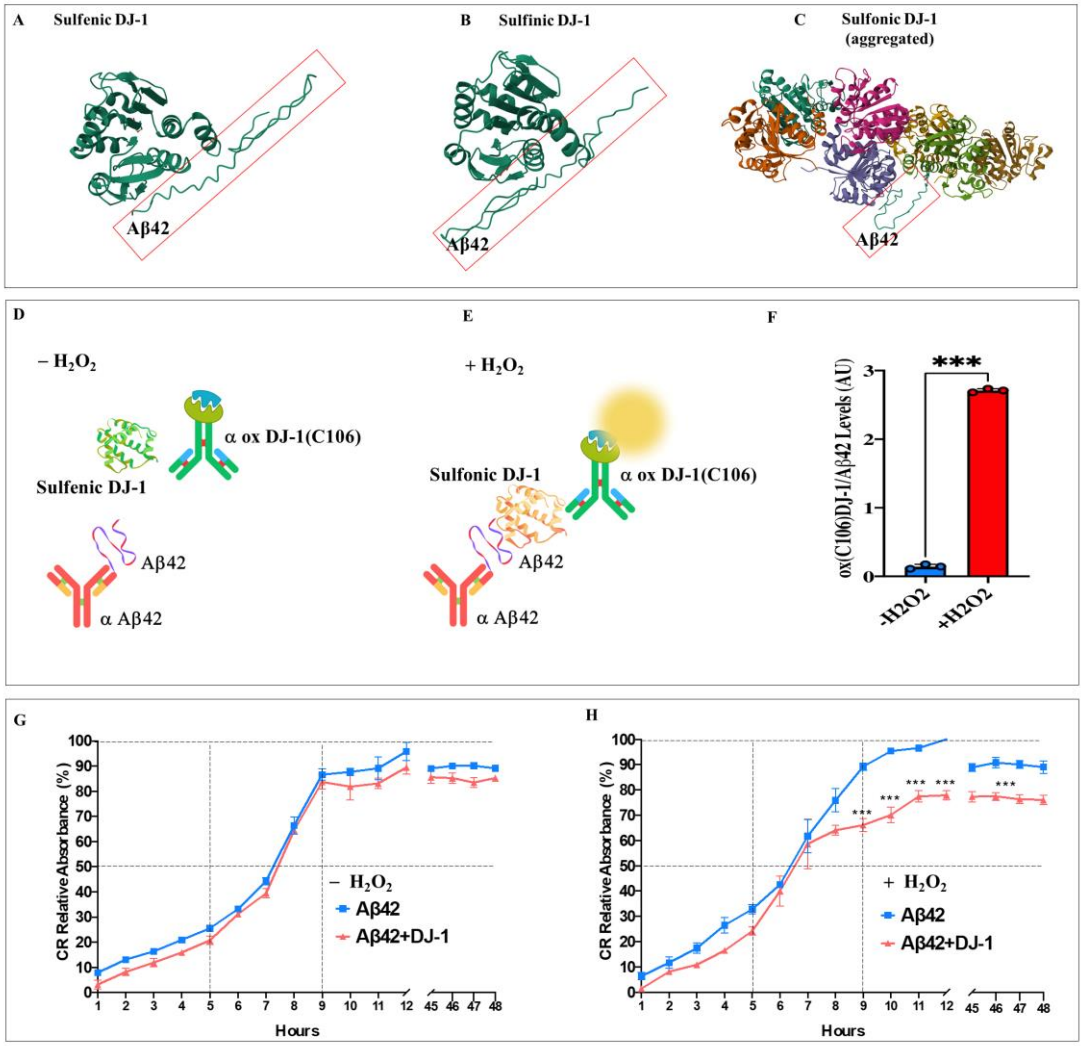

Figure 7. In silico docking analysis of the binding of sulfonic DJ-1 (Cys^{106}-SO_3) and monomeric amyloid beta 42 (A 42), ELISA test, and fibril growth in cell-free analysis. Representative HDOCK 3D images showing the molecular docking of (A) Sulfenic (PDB:4p34), (B) Sulfinic (PDB: 1soa), (C) sulfonic DJ-1 (aggregated, PDB: 3bwe) with monomeric A 42. (D) ELISA test diagram of A 42 and DJ-1 in the absence of H2O2; (E) ELISA test diagram of A 42 and DJ-1 in the presence of H2O2; (F) Quantification of the levels of ox(106) DJ-1-A 42 levels in absence or presence of H2O2. (G) Representative aggregation kinetics of A 42 fibrillar growth in presence of DJ-1 and the absence of H_2O_2. (H) Representative aggregation kinetics of A 42 fibrillar growth in presence of DJ-1 and in the presence of H_2O_2. The figures represent 1 out of 3 independent experiments (n = 3). Data are expressed as mean ± SD; ***p < 0.001; ns = not significant. Figures/histograms, and bars represent 1 of 3 independent experiments (n = 3).

 doi:10.20944/preprints202511.1634.v1

4. Discussion

In the present study, we demonstrate that sulfonated DJ-1 (DJ-1 Cys^{106}-SO_3H) colocalizes with intracellular $A\beta_{42}$ in cells from the hippocampi and frontal and occipital cortices of brains of patients with FAD caused by the PSEN1 E280A mutation. These findings contradict those of Solti et al. [46]**.** While those authors suggest that oxidized DJ-1 aggregates colocalize with amyloid deposits in the frontal cortex of human SAD patients, we found intracellular accumulation of Aβ42 and DJ-1 in brain cells (**see Figure 5**). One possible explanation for this discrepancy is the different antibodies used to detect Aβ. The Solti's group used a polyclonal rabbit antibody (Abcam, Cat# ab2539) raised against human APP, whereas we used a monoclonal anti-β-amyloid antibody (BioLegend, Clone 6E10, Cat# 803014, RRID: AB_2728527). Interestingly, we detected the colocalization of DJ-1 and Aβ42 in blood vessels for the first time in FAD brain samples (**Figure 1T**). This observation suggests that not only do DJ-1 and Aβ42 proteins aggregate in neuronal cells, but endothelial cells are also capable of accumulating and aggregating intracellular Aβ42 [51] and oxidized DJ-1. Consequently, the positive identification of sulfonic DJ-1 and Aβ42 should be considered a marker of cerebral amyloid angiopathy (CAA) in FAD brain pathology. However, it remains unclear whether PSEN1 E280A neurons accumulate and aggregate intracellular Aβ by a similar mechanism as endothelial cells [52], a question that deserves further investigation. We also present evidence of the concurrent accumulation of iAβ and oxidized DJ-1 in PSEN1 E280A iPSC-derived cerebral organoids neurons (COs) and NPC-derived cholinergic neurons (ChNs). Similar proteinaceous pathology was also observed in MSCs/MenSCs PSEN1 E280A-derived ChLNs and cerebral spheroids [31,53,54] or PSEN1 I416T ChLNs derived from MenSCs [28]. These observations suggest that the colocalization of DJ-1 with Aβ42 occurs independently of the cells' pluripotent or stromal origin. Furthermore, both proteins appear to colocalize simultaneously in the early stages of cholinergic lineage development (e.g., [27,31]). However, the nature of their colocalization remains unclear i.e., are they accidental encounters or partners? Our findings support the notion that A 42 and oxidized DJ-1 are associates proteins.

In silico molecular docking analysis suggest that sulfonic DJ-1 physically interacts with iAβ42. Such theoretical prediction was confirmed by ELISA test and RT-QuIC. According to ELISA test, sulfonic DJ-1, but not reduced DJ-1, binds to A 42. Likewise, RT-QuIC experiments show that sulfonic DJ-1, but not reduced DJ-1, was able to bind to monomeric iAβ42. In fact, in the RT-QuIC test, sulfonic DJ-1 significantly reduced Aβ42 fibril formation during the plateau phase, likely due to a shortage of available monomeric Aβ. Since sulfonic DJ-1 did not interfere with the growth phase of Aβ fibrils, these results suggest that DJ-1 binds to iAβ42 in a noncovalent manner. Interestingly, sulfonic DJ-1 has been shown to form aggregates not only with Aβ but also with α-synuclein (α-Syn) and p-Thr205 tau, intraneuronal pathogenic proteins involved in PD and AD, respectively [46]. Unexpectedly, these DJ-1-protein complexes (Aβ, α-synuclein, and p-Tau) may overwhelm the autophagy-lysosomal pathway, an efficient protein degradation system most impaired in AD [31,55]. Further investigation is needed to determine if sulfonic DJ-1 physically interacts with α-synuclein and p-Tau, as demonstrated in the present study with Aβ42.

Our findings support the intracellular amyloid hypothesis [23,24]. Indeed, we (e.g., [27,28] and others [56–63] have provided evidence for the intracellular accumulation of Aβ within neurons, including studies on postmortem AD brains, transgenic mouse brains, and in vitro AD models. Recently, we have demonstrated that, during the transdifferentiation of mesenchymal stromal cells (MenSCs) into the PSEN1 E280A cholinergic lineage, the production and accumulation of the iAβ42 fragment increased after seven days of transdifferentiation of the PSEN1 E280A ChLNs compared to day zero of transdifferentiation [31]. In parallel, we observed a significant increase in DJ-1C^{106}-SO_3 at day 7 and an increase in autophagosome accumulation at day 5 of transdifferentiation, though there were no detected cell death markers. These observations suggest that the earliest pathological events in PSEN1 E280A ChLNs are the simultaneous accumulation of iAβ42, sulfonic DJ-1 (Cys^{106}-SO_3), and autophagosomes [31]. Since antioxidant agents (e.g., EGCG and tramiprosate) abolished these molecular events in mutant ChLNs, we suspected a link between them. However, the mechanism by

 doi:10.20944/preprints202511.1634.v1

which iA , DJ-1 Cys^{106}-SO$_3$, and autophagosomes interact has not been clearly delineated. One possible explanation is that PSEN1 E280A-overproduced iA 42 generates H_2O_2 through direct or indirect inhibition of mitochondrial complex I [64,65]. Since DJ-1 is an atypical peroxiredoxin-like peroxidase that scavenges H_2O_2 through oxidation of Cys^{106}-SH [66], this molecule can turn sulfenic acid (Cys^{106}-SOH) into sulfonic acid groups (Cys^{106}-SO$_3$H) in DJ-1 protein [37,67], leading to loss of function and protein aggregation [42]. Interestingly, sulfonic acid DJ-1 (Cys^{106}-SO$_3$) can form a protein complex with iA 42 (this work), which possibly overcharged the autophagy-lysosomal pathway, wherein the autophagosomes accumulate and fail to mature into functional autolysosomes [68], leading to a blockage in the degradation process in mutant ChLNs. Therefore, early suppression of H_2O_2 generation (e.g., by antioxidants) might block the cascade of events, such iA 42> mitochondria Complex I > H_2O_2> DJ-1 (Cys^{106}-SO$_3$)>> iA 42-sulfonic DJ-1 complex, leading to dysregulation of autophagy. Our present work and previous one (e.g., [27,31]) supports such a scenario (**Figure 8)**.

5. Conclusions

We have consistently observed the simultaneous presence of Aβ42 and oxidized DJ-1 in PSEN1 E280A postmortem brain tissue, including the frontal and occipital cortices and the hippocampus, as well as in cerebral organoids derived from PSEN1 E280A induced pluripotent stem cells (iPSCs) and neuronal precursor cell-derived cholinergic neurons. An in silico molecular analysis predicted that sulfonic DJ-1 might bind to Aβ42. The ELISA test and RT-QuIC findings corroborated this assumption. Taken together, these observations suggest that the colocalization of Aβ42 and DJ-1 in pathological tissue, organoids, or cells may be due to a physical interaction between the two proteins. Based on previous findings by our group [27,31] and this study, **Figure 8** illustrates a potential mechanism by which oxidized DJ-1 and Aβ42 protein complexes may impair the autophagy-lysosome system and cause neuronal death.

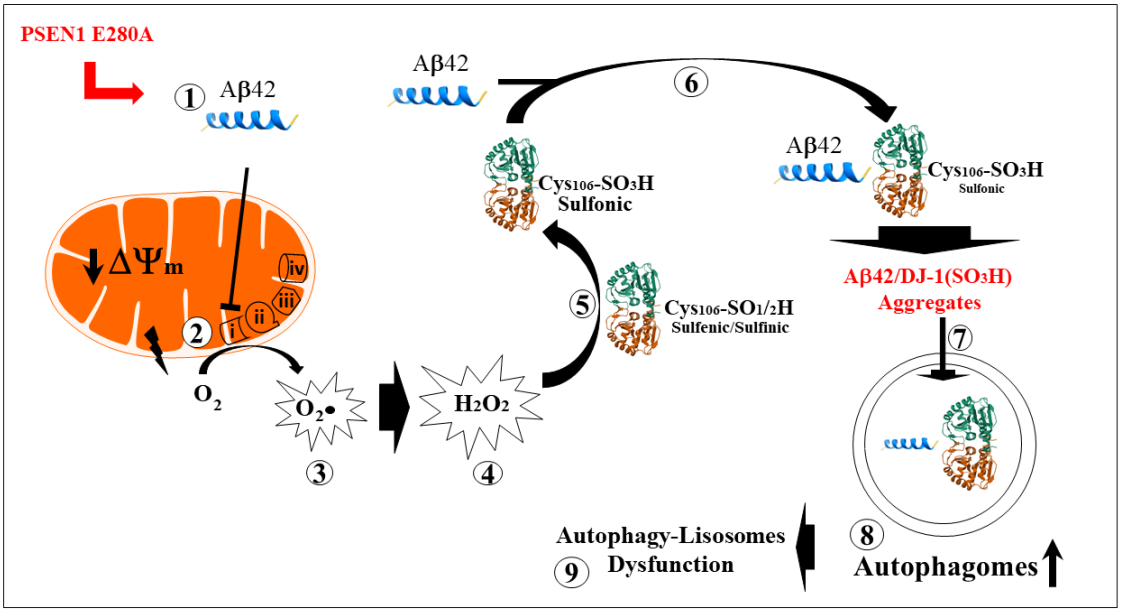

Figure 8. Schematic representation of the early intraneuronal pathological interactions between Aβ42 and oxidized DJ-1. (**1**) PSEN1 E280A-induced monomeric intracellular Aβ42 production is imported into the mitochondria via the translocase of the outer membrane (TOM) import machinery [69]. (**2**) Once inside the mitochondrial matrix, Aβ42 binds to and blocks Complex I, resulting in electron leakage [64,65]. This is followed by non-enzymatic reactions involving the one-electron reduction of molecular oxygen into superoxide anion radicals (**3**). These radicals can then be converted to hydrogen peroxide (H_2O_2, step **4**) through a dismutation reaction, either spontaneously or catalyzed by the enzyme superoxide dismutase (SOD). (**5**) The H_2O_2 then oxidizes sulfenic (-SOH) to sulfinic (-SO$_2$H) to sulfonic (-SO$_3$H) DJ-1, which physically binds to Aβ42 (**6**, this

 doi:10.20944/preprints202511.1634.v1

work), forming Aβ42-DJ-1 Cys106-SO_3H aggregates (**7**, this work). In an attempt to eliminate these aggregates, Aβ42-DJ-1 complex accumulates in autophagosomes (**8**). Because the autophagy-lysosomal system is unable to clear these aggregates efficiently, the autophagosomes accumulate [31]. This may contribute to impairment of the autophagy-lysosomal pathway (**9**) and, over time, cell death.

Author Contributions: Author Contributions. Conceptualization, C.V.-P, and M.J.Del-R.; methodology, V.S.-M., and M.M.-P.; formal analysis, V.S.-M., and M.M.-P.; validation: V.S.-M. and M.M.-P.; investigation, C.V.-P., and M.J.Del-R.; resources, M.J.Del-R.; data curation, V.S.-M., and M.M.-P.; writing—original draft preparation, C.V.-P, and M.J. Del-R.; writing—review and editing, V.S.-M., M.M.-P.; C.V.-P., and M.J. Del-R.; supervision, M.M.-P.; project administration, M.J. Del -R.; funding acquisition, M.J. Del-R. and V.S.M. All authors have read and agreed to the published version of the manuscript.

Funding: This research was funded by the National Institute on Aging, grant # 1RF1AG062479-01 and Minciencias - Programa Orquídeas, mujeres en la ciencia 2024 (948) contract 112721-201-2024.

Human: Ethics: Not applicable.

Consent to Participate: Informed consent was obtained from all individual participants included in the study.

Availability of Data and Material: All datasets generated for this study are included in the manuscript.

Acknowledgments: We would like to acknowledge the National Institute on Aging for the grant,number 1RF1AG062479-01, awarded to Kenneth S. Kosik at the University of California, Santa Barbara, CA, USA, as the principal investigator. This work is dedicated to Francisco Lopera (1951–2024). .

Conflict of Interest: The authors declare no competing interests.

Declarations: Ethical Approval Menstrual specimen donors provided a signed informed consent approved by the ethics committee of the Sede de Investigación Universitaria (SIU), University of Antioquia, Medellín, Colombia (Act 23-10-854).

Authors' information: V.S.-M. is postdoctoral researcher at the University of Antioquia (UdeA). M.M.-P., C.V.-P. and M.J.DelR are associated and senior professors, respectively, at the University of Antioquia.

Consent for Publication: Not applicable.

References

1. Mendez, M.F. Early-Onset Alzheimer Disease. *Neurol Clin* 2017, *35*, 263–281, doi:10.1016/J.NCL.2017.01.005.
2. Mendez, M.F. Early-Onset Alzheimer Disease and Its Variants. *Continuum (Minneap Minn)* 2019, *25*, 34–51, doi:10.1212/CON.0000000000000687.
3. Doher, N.; Davoudi, V.; Magaki, S.; Townley, R.A.; Haeri, M.; Vinters, H. V. Illustrated Neuropathologic Diagnosis of Alzheimer's Disease. *Neurol Int* 2023, *15*, 857–867, doi:10.3390/NEUROLINT15030054.
4. Miao, Y.; Wolfe, M.S. Emerging Structures and Dynamic Mechanisms of γ-Secretase for Alzheimer's Disease. *Neural Regen Res* 2025, *20*, 174–180, doi:10.4103/NRR.NRR-D-23-01781.
5. Johnson, D.S.; Li, Y.M.; Pettersson, M.; St George-Hyslop, P.H. Structural and Chemical Biology of Presenilin Complexes. *Cold Spring Harb Perspect Med* 2017, *7*, 25, doi:10.1101/CSHPERSPECT.A024067.
6. Steiner, H.; Fukumori, A.; Tagami, S.; Okochi, M. Making the Final Cut: Pathogenic Amyloid-β Peptide Generation by γ-Secretase. *Cell Stress* 2018, *2*, 292–310, doi:10.15698/CST2018.11.162.
7. Hardy, J.A.; Higgins, G.A. Alzheimer's Disease: The Amyloid Cascade Hypothesis. *Science* 1992, *256*, 184–185, doi:10.1126/SCIENCE.1566067.
8. Whitehouse, P.J.; Price, D.L.; Struble, R.G.; Clark, A.W.; Coyle, J.T.; DeLong, M.R. Alzheimer's Disease and Senile Dementia: Loss of Neurons in the Basal Forebrain. *Science* 1982, *215*, 1237–1239, doi:10.1126/SCIENCE.7058341.
9. Markesbery, W.R. Oxidative Stress Hypothesis in Alzheimer's Disease. *Free Radic Biol Med* 1997, *23*, 134–147, doi:10.1016/S0891-5849(96)00629-6.

10. Zhu, X.; Raina, A.K.; Perry, G.; Smith, M.A. Alzheimer's Disease: The Two-Hit Hypothesis. *Lancet Neurology* 2004, *3*, 219–226, doi:10.1016/S1474-4422(04)00707-0.
11. Swerdlow, R.H.; Khan, S.M. A "Mitochondrial Cascade Hypothesis" for Sporadic Alzheimer's Disease. *Med Hypotheses* 2004, *63*, 8–20, doi:10.1016/j.mehy.2003.12.045.
12. Shen, J.; Kelleher, R.J. The Presenilin Hypothesis of Alzheimer's Disease: Evidence for a Loss-of-Function Pathogenic Mechanism. *Proc Natl Acad Sci U S A* 2007, *104*, 403–409, doi:10.1073/PNAS.0608332104.
13. Pensalfini, A.; Albay, R.; Rasool, S.; Wu, J.W.; Hatami, A.; Arai, H.; Margol, L.; Milton, S.; Poon, W.W.; Corrada, M.M.; et al. Intracellular Amyloid and the Neuronal Origin of Alzheimer Neuritic Plaques. *Neurobiol Dis* 2014, *71*, 53–61, doi:10.1016/J.NBD.2014.07.011.
14. Gouras, G.K.; Willén, K.; Faideau, M. The Inside-out Amyloid Hypothesis and Synapse Pathology in Alzheimer's Disease. *Neurodegener Dis* 2014, *13*, 142–146, doi:10.1159/000354776.
15. Arnsten, A.F.T.; Datta, D.; Del Tredici, K.; Braak, H. Hypothesis: Tau Pathology Is an Initiating Factor in Sporadic Alzheimer's Disease. *Alzheimers Dement* 2021, *17*, 115–124, doi:10.1002/ALZ.12192.
16. Martens, Y.A.; Zhao, N.; Liu, C.C.; Kanekiyo, T.; Yang, A.J.; Goate, A.M.; Holtzman, D.M.; Bu, G. ApoE Cascade Hypothesis in the Pathogenesis of Alzheimer's Disease and Related Dementias. *Neuron* 2022, *110*, 1304–1317, doi:10.1016/j.neuron.2022.03.004.
17. Agarwal, M.; Alam, M.R.; Haider, M.K.; Malik, M.Z.; Kim, D.K. Alzheimer's Disease: An Overview of Major Hypotheses and Therapeutic Options in Nanotechnology. *Nanomaterials (Basel)* 2020, *11*, 1–18, doi:10.3390/NANO11010059.
18. Bermejo-Pareja, F.; del Ser, T. Controversial Past, Splendid Present, Unpredictable Future: A Brief Review of Alzheimer Disease History. *J Clin Med* 2024, *13*, doi:10.3390/JCM13020536.
19. Chen, Z.R.; Huang, J.B.; Yang, S.L.; Hong, F.F. Role of Cholinergic Signaling in Alzheimer's Disease. *Molecules* 2022, *27*, doi:10.3390/MOLECULES27061816.
20. Kepp, K.P.; Robakis, N.K.; Høilund-Carlsen, P.F.; Sensi, S.L.; Vissel, B. The Amyloid Cascade Hypothesis: An Updated Critical Review. *Brain* 2023, *146*, 3969–3990, doi:10.1093/BRAIN/AWAD159.
21. Behl, C. In 2024, the Amyloid-Cascade-Hypothesis Still Remains a Working Hypothesis, No Less but Certainly No More. *Front Aging Neurosci* 2024, *16*, doi:10.3389/FNAGI.2024.1459224/PDF.
22. Almohmadi, N.H.; Al-Kuraishy, H.M.; Albuhadily, A.K.; Al-Gareeb, A.I.; Abdelaziz, A.M.; Alexiou, A.; Papadakis, M.; El-Saber Batiha, G. Alzheimer Disease: Amyloid Peptide Controversies and Challenges of Anti-Aβ Immunotherapy. *Journal of Pharmacology and Experimental Therapeutics* 2025, *392*, doi:10.1016/j.jpet.2025.103639.
23. Li, M.; Chen, L.; Lee, D.H.S.; Yu, L.C.; Zhang, Y. The Role of Intracellular Amyloid β in Alzheimer's Disease. *Prog Neurobiol* 2007, *83*, 131–139, doi:10.1016/j.pneurobio.2007.08.002.
24. Okazawa, H. Intracellular Amyloid Hypothesis for Ultra-Early Phase Pathology of Alzheimer's Disease. *Neuropathology* 2021, *41*, 93–98, doi:10.1111/NEUP.12738.
25. Lalli, M.A.; Cox, H.C.; Arcila, M.L.; Cadavid, L.; Moreno, S.; Garcia, G.; Madrigal, L.; Reiman, E.M.; Arcos-Burgos, M.; Bedoya, G.; et al. Origin of the PSEN1 E280A Mutation Causing Early-Onset Alzheimer's Disease. *Alzheimers Dement* 2014, *10*, S277-S283.e10, doi:10.1016/J.JALZ.2013.09.005.
26. Ramirez Aguilar, L.; Acosta-Uribe, J.; Giraldo, M.M.; Moreno, S.; Baena, A.; Alzate, D.; Cuastumal, R.; Aguillón, D.; Madrigal, L.; Saldarriaga, A.; et al. Genetic Origin of a Large Family with a Novel PSEN1 Mutation (Ile416Thr). *Alzheimers Dement* 2019, *15*, 709–719, doi:10.1016/J.JALZ.2018.12.010.
27. Soto-Mercado, V.; Mendivil-Perez, M.; Velez-Pardo, C.; Lopera, F.; Jimenez-Del-Rio, M. Cholinergic-like Neurons Carrying PSEN1 E280A Mutation from Familial Alzheimer's Disease Reveal Intraneuronal SAPPβ Fragments Accumulation, Hyperphosphorylation of TAU, Oxidative Stress, Apoptosis and Ca2+ Dysregulation: Therapeutic Implications. *PLoS One* 2020, *15*, doi:10.1371/journal.pone.0221669.
28. Gomez-Sequeda, N.; Mendivil-Perez, M.; Jimenez-Del-Rio, M.; Lopera, F.; Velez-Pardo, C. Cholinergic-like Neurons and Cerebral Spheroids Bearing the PSEN1 p.Ile416Thr Variant Mirror Alzheimer's Disease Neuropathology. *Sci Rep* 2023, *13*, doi:10.1038/S41598-023-39630-4.
29. Mendivil-Perez, M.; Velez-Pardo, C.; Lopera, F.; Kosik, K.S.; Jimenez-Del-Rio, M. PSEN1 E280A Cholinergic-like Neurons and Cerebral Spheroids Derived from Mesenchymal Stromal Cells and from

 doi:10.20944/preprints202511.1634.v1

Induced Pluripotent Stem Cells Are Neuropathologically Equivalent. *Int J Mol Sci* 2023, *24*, doi:10.3390/ijms24108957.

30. Mendivil-Perez, M.; Velez-Pardo, C.; Jimenez-Del-Rio, M. Direct Transdifferentiation of Human Wharton's Jelly Mesenchymal Stromal Cells into Cholinergic-like Neurons. *J Neurosci Methods* 2019, *312*, 126–138, doi:10.1016/j.jneumeth.2018.11.019.
31. Soto-Mercado, V.; Mendivil-Perez, M.; Jimenez-Del-Rio, M.; Velez-Pardo, C. Combination of Epigallocatechin-3-Gallate and Tramiprosate Prevent Accumulation of Intracellular Aβ and Dysfunctional Autophagy-Lysosomal Pathway at Earliest Stage of Transdifferentiation of Mesenchymal Stromal Cells into PSEN1 E280A Cholinergic-like Neu…. *Int J Mol Sci* 2025, *26*, doi:10.3390/IJMS26083756.
32. Bloom, G.S. Amyloid-β and Tau: The Trigger and Bullet in Alzheimer Disease Pathogenesis. *JAMA Neurol* 2014, *71*, 505–508, doi:10.1001/JAMANEUROL.2013.5847.
33. Villarejo, L.G.; Bachmann, L.; Marks, D.; Brachthäuser, M.; Geidies, A.; Müller, T. Role of Intracellular Amyloid β as Pathway Modulator, Biomarker, and Therapy Target. *Int J Mol Sci* 2022, *23*, doi:10.3390/IJMS23094656.
34. Bonifati, V.; Rizzu, P.; Van Baren, M.J.; Schaap, O.; Breedveld, G.J.; Krieger, E.; Dekker, M.C.J.; Squitieri, F.; Ibanez, P.; Joosse, M.; et al. Mutations in the DJ-1 Gene Associated with Autosomal Recessive Early-Onset Parkinsonism. *Science* 2003, *299*, 256–259, doi:10.1126/SCIENCE.1077209.
35. Smith, N.; Wilson, M.A. Structural Biology of the DJ-1 Superfamily. *Adv Exp Med Biol* 2017, *1037*, 5–24, doi:10.1007/978-981-10-6583-5_2.
36. Neves, M.; Grãos, M.; Anjo, S.I.; Manadas, B. Modulation of Signaling Pathways by DJ-1: An Updated Overview. *Redox Biol* 2022, *51*, doi:10.1016/j.redox.2022.102283.
37. Kinumi, T.; Kimata, J.; Taira, T.; Ariga, H.; Niki, E. Cysteine-106 of DJ-1 Is the Most Sensitive Cysteine Residue to Hydrogen Peroxide-Mediated Oxidation in Vivo in Human Umbilical Vein Endothelial Cells. *Biochem Biophys Res Commun* 2004, *317*, 722–728, doi:10.1016/j.bbrc.2004.03.110.
38. Taira, T.; Saito, Y.; Niki, T.; Iguchi-Ariga, S.M.M.; Takahashi, K.; Ariga, H. DJ-1 Has a Role in Antioxidative Stress to Prevent Cell Death. *EMBO Rep* 2004, *5*, 213–218, doi:10.1038/SJ.EMBOR.7400074.
39. Canet-Avilés, R.M.; Wilson, M.A.; Miller, D.W.; Ahmad, R.; McLendon, C.; Bandyopadhyay, S.; Baptista, M.J.; Ringe, D.; Petsko, G.A.; Cookson, M.R. The Parkinson's Disease Protein DJ-1 Is Neuroprotective Due to Cysteine-Sulfinic Acid-Driven Mitochondrial Localization. *Proc Natl Acad Sci U S A* 2004, *101*, 9103–9108, doi:10.1073/PNAS.0402959101.
40. Raninga, P. V.; Di Trapani, G.; Tonissen, K.F. The Multifaceted Roles of DJ-1 as an Antioxidant. *Adv Exp Med Biol* 2017, *1037*, 67–87, doi:10.1007/978-981-10-6583-5_6.
41. Wilson, M.A. The Role of Cysteine Oxidation in DJ-1 Function and Dysfunction. *Antioxid Redox Signal* 2011, *15*, 111, doi:10.1089/ARS.2010.3481.
42. Kiss, R.; Zhu, M.; Jójárt, B.; Czajlik, A.; Solti, K.; Fórizs, B.; Nagy, É.; Zsila, F.; Beke-Somfai, T.; Tóth, G. Structural Features of Human DJ-1 in Distinct Cys106 Oxidative States and Their Relevance to Its Loss of Function in Disease. *Biochim Biophys Acta Gen Subj* 2017, *1861*, 2619–2629, doi:10.1016/J.BBAGEN.2017.08.017.
43. Ariga, H.; Iguchi-Ariga, S.M.M. Introduction/Overview. *Adv Exp Med Biol* 2017, *1037*, 1–4, doi:10.1007/978-981-10-6583-5_1.
44. Choi, J.; Sullards, M.C.; Olzmann, J.A.; Rees, H.D.; Weintraub, S.T.; Bostwick, D.E.; Gearing, M.; Levey, A.I.; Chin, L.S.; Li, L. Oxidative Damage of DJ-1 Is Linked to Sporadic Parkinson and Alzheimer Diseases. *J Biol Chem* 2006, *281*, 10816, doi:10.1074/JBC.M509079200.
45. Baulac, S.; Lu, H.; Strahle, J.; Yang, T.; Goldberg, M.S.; Shen, J.; Schlossmacher, M.G.; Lemere, C.A.; Lu, Q.; Xia, W. Increased DJ-1 Expression under Oxidative Stress and in Alzheimer's Disease Brains. *Mol Neurodegener* 2009, *4*, doi:10.1186/1750-1326-4-12.
46. Solti, K.; Kuan, W.L.; Fórizs, B.; Kustos, G.; Mihály, J.; Varga, Z.; Herberth, B.; Moravcsik, É.; Kiss, R.; Kárpáti, M.; et al. DJ-1 Can Form β-Sheet Structured Aggregates That Co-Localize with Pathological Amyloid Deposits. *Neurobiol Dis* 2020, *134*, 104629, doi:10.1016/J.NBD.2019.104629.
47. Soto-Mercado, V.; Mendivil-Perez, M.; Velez-Pardo, C.; Jimenez-Del-Rio, M. Neuroprotective Effect of Combined Treatment with Epigallocatechin 3-Gallate and Melatonin on Familial Alzheimer's Disease

 doi:10.20944/preprints202511.1634.v1

PSEN1 E280A Cerebral Spheroids Derived from Menstrual Mesenchymal Stromal Cells. *Journal of Alzheimer's Disease* 2024, *99*, S51–S66, doi:10.3233/JAD-220903.

48. Klunk, W.E.; Jacob, R.F.; Mason, R.P. Quantifying Amyloid by Congo Red Spectral Shift Assay. *Methods Enzymol* 1999, *309*, 285–305, doi:10.1016/S0076-6879(99)09021-7.
49. Lazic, S.E.; Clarke-Williams, C.J.; Munafò, M.R. What Exactly Is 'N' in Cell Culture and Animal Experiments? *PLoS Biol* 2018, *16*, doi:10.1371/journal.pbio.2005282.
50. Velez-Pardo, C.; Lopera, F.; Jimenez Del Rio, M. DNA Damage Does Not Correlate with Amyloid-Beta-Plaques and Neurofibrillary Tangles in Familial Alzheimer's Disease Presenilin-1 [E280A] Mutation. *J Alzheimers Dis* 2000, *2*, 47–57, doi:10.3233/JAD-2000-2106.
51. Tachida, Y.; Miura, S.; Muto, Y.; Takuwa, H.; Sahara, N.; Shindo, A.; Matsuba, Y.; Saito, T.; Taniguchi, N.; Kawaguchi, Y.; et al. Endothelial Expression of Human Amyloid Precursor Protein Leads to Amyloid β in the Blood and Induces Cerebral Amyloid Angiopathy in Knock-in Mice. *Journal of Biological Chemistry* 2022, *298*, doi:10.1016/j.jbc.2022.101880.
52. Nishikage, S.; Fujisawa, A.; Endoh, H.; Sakamoto, H.; Suzuki, T.; Kanzawa, M.; Ishii, S.; Okano, M.; Nitta, E.; Yakushijin, K.; et al. Amyloid Deposition through Endocytosis in Vascular Endothelial Cells. *Exp Hematol* 2024, *129*, doi:10.1016/j.exphem.2023.11.003.
53. Soto-Mercado, V.; Mendivil-Perez, M.; Velez-Pardo, C.; Jimenez-Del-Rio, M. Neuroprotective Effect of Combined Treatment with Epigallocatechin 3-Gallate and Melatonin on Familial Alzheimer's Disease PSEN1 E280A Cerebral Spheroids Derived from Menstrual Mesenchymal Stromal Cells. *J Alzheimers Dis* 2024, *99*, S51–S66, doi:10.3233/JAD-220903.
54. Mendivil-Perez, M.; Velez-Pardo, C.; Lopera, F.; Kosik, K.S.; Jimenez-Del-Rio, M. PSEN1 E280A Cholinergic-like Neurons and Cerebral Spheroids Derived from Mesenchymal Stromal Cells and from Induced Pluripotent Stem Cells Are Neuropathologically Equivalent. *Int J Mol Sci* 2023, *24*, doi:10.3390/IJMS24108957.
55. Zhang, W.; Xu, C.; Sun, J.; Shen, H.M.; Wang, J.; Yang, C. Impairment of the Autophagy–Lysosomal Pathway in Alzheimer's Diseases: Pathogenic Mechanisms and Therapeutic Potential. *Acta Pharm Sin B* 2022, *12*, 1019, doi:10.1016/J.APSB.2022.01.008.
56. Grundke-Iqbal, I.; Iqbal, K.; George, L.; Tung, Y.C.; Kim, K.S.; Wisniewski, H.M. Amyloid Protein and Neurofibrillary Tangles Coexist in the Same Neuron in Alzheimer Disease. *Proc Natl Acad Sci U S A* 1989, *86*, 2853–2857, doi:10.1073/PNAS.86.8.2853.
57. LaFerla, F.M.; Green, K.N.; Oddo, S. Intracellular Amyloid-Beta in Alzheimer's Disease. *Nat Rev Neurosci* 2007, *8*, 499–509, doi:10.1038/NRN2168.
58. Wirths, O.; Bayer, T.A. Intraneuronal Aβ Accumulation and Neurodegeneration: Lessons from Transgenic Models. *Life Sci* 2012, *91*, 1148–1152, doi:10.1016/J.LFS.2012.02.001.
59. Takahashi, R.H.; Nagao, T.; Gouras, G.K. Plaque Formation and the Intraneuronal Accumulation of β-Amyloid in Alzheimer's Disease. *Pathol Int* 2017, *67*, 185–193, doi:10.1111/PIN.12520.
60. Welikovitch, L.A.; Do Carmo, S.; Maglóczky, Z.; Szocsics, P.; Lőke, J.; Freund, T.; Cuello, A.C. Evidence of Intraneuronal Aβ Accumulation Preceding Tau Pathology in the Entorhinal Cortex. *Acta Neuropathol* 2018, *136*, 901–917, doi:10.1007/S00401-018-1922-Z.
61. Roos, T.T.; Garcia, M.G.; Martinsson, I.; Mabrouk, R.; Israelsson, B.; Deierborg, T.; Kobro-Flatmoen, A.; Tanila, H.; Gouras, G.K. Neuronal Spreading and Plaque Induction of Intracellular Aβ and Its Disruption of Aβ Homeostasis. *Acta Neuropathol* 2021, *142*, 669–687, doi:10.1007/S00401-021-02345-9.
62. Kobro-Flatmoen, A.; Hormann, T.M.; Gouras, G. Intracellular Amyloid-β in the Normal Rat Brain and Human Subjects and Its Relevance for Alzheimer's Disease. *J Alzheimers Dis* 2023, *95*, 719–733, doi:10.3233/JAD-230349.
63. Yeapuri, P.; Machhi, J.; Foster, E.G.; Kadry, R.; Bhattarai, S.; Lu, Y.; Sil, S.; Sapkota, R.; Srivastava, S.; Kumar, M.; et al. Amyloid Precursor Protein and Presenilin-1 Knock-in Immunodeficient Mice Exhibit Intraneuronal Aβ Pathology, Microgliosis, and Extensive Neuronal Loss. *Alzheimers Dement* 2025, *21*, doi:10.1002/ALZ.70084.

 doi:10.20944/preprints202511.1634.v1

64. Bobba, A.; Amadoro, G.; Valenti, D.; Corsetti, V.; Lassandro, R.; Atlante, A. Mitochondrial Respiratory Chain Complexes I and IV Are Impaired by β-Amyloid via Direct Interaction and through Complex I-Dependent ROS Production, Respectively. *Mitochondrion* 2013, *13*, 298–311, doi:10.1016/j.mito.2013.03.008.
65. Atlante, A.; Valenti, D. Mitochondrial Complex I and β-Amyloid Peptide Interplay in Alzheimer's Disease: A Critical Review of New and Old Little Regarded Findings. *Int J Mol Sci* 2023, *24*, doi:10.3390/IJMS242115951.
66. Andres-Mateos, E.; Perier, C.; Zhang, L.; Blanchard-Fillion, B.; Greco, T.M.; Thomas, B.; Han, S.K.; Sasaki, M.; Ischiropoulos, H.; Przedborski, S.; et al. DJ-1 Gene Deletion Reveals That DJ-1 Is an Atypical Peroxiredoxin-like Peroxidase. *Proc Natl Acad Sci U S A* 2007, *104*, 14807–14812, doi:10.1073/PNAS.0703219104.
67. Miyama, A.; Saito, Y.; Yamanaka, K.; Hayashi, K.; Hamakubo, T.; Noguchi, N. Oxidation of DJ-1 Induced by 6-Hydroxydopamine Decreasing Intracellular Glutathione. *PLoS One* 2011, *6*, e27883, doi:10.1371/JOURNAL.PONE.0027883.
68. Zhang, J. Teaching the Basics of Autophagy and Mitophagy to Redox Biologists--Mechanisms and Experimental Approaches. *Redox Biol* 2015, *4*, 242–259, doi:10.1016/J.REDOX.2015.01.003.
69. Hansson Petersen, C.A.; Alikhani, N.; Behbahani, H.; Wiehager, B.; Pavlov, P.F.; Alafuzoff, I.; Leinonen, V.; Ito, A.; Winblad, B.; Glaser, E.; et al. The Amyloid Beta-Peptide Is Imported into Mitochondria via the TOM Import Machinery and Localized to Mitochondrial Cristae. *Proc Natl Acad Sci U S A* 2008, *105*, 13145–13150, doi:10.1073/PNAS.0806192105.